2. EXPLANATORY NOTES[1]

Shipboard Scientific Party[2]

INTRODUCTION

In this chapter, we have assembled information that will help the reader understand the observations on which our preliminary conclusions are based and also help the interested investigator select samples for further analysis. This information concerns only shipboard operations and analyses described in the site reports in the *Initial Reports* volume of the Leg 151 *Proceedings of the Ocean Drilling Program*. Methods used by various investigators for shore-based analyses of Leg 151 data will be described in the individual scientific contributions to be published in the *Scientific Results* volume.

Authorship of Site Chapters

The separate sections of the site chapters were written by the following shipboard scientists (authors are listed in alphabetical order, no seniority is implied):

Site Summary: Myhre, Thiede
Background and Objectives: Myhre, Thiede
Operations: Firth, Pollard
Lithostratigraphy: Ahagon, Chow, Cremer, Flower, Fronval, McManus, O'Connell, Wolf-Welling
Biostratigraphy: Firth, Hull, Koç, Osterman, Sato, Scherer, Spiegler
Paleomagnetism: Williamson, Witte
Igneous Petrology: Davis
Organic Geochemistry: Stein
Inorganic Geochemistry: Brass
Physical Properties: Black, Bloemendal, Hood, Larsen, Rack
Downhole Measurements: Bristow, Lyle
Seismic Stratigraphy: Lyle
Stratigraphic Correlations: Bloemendal

In an appendix following the site chapters are summary core descriptions ("barrel sheets") and photographs of each core.

ODP is in the process of replacing the bulk of the Explanatory Notes in each *Initial Reports* volume with "Annual Explanatory Notes to Initial Reports Volumes." These complete, detailed, and annually updated notes will reduce redundancy. In anticipation of this change, we have omitted some of the general information that has been reprinted repeatedly in past *Initial Reports* volumes. Reference is made to other *Initial Reports* volumes for detailed description of methods if appropriate.

Drilling Operations

Three coring systems were used during Leg 151: the advanced hydraulic piston corer (APC), the extended core barrel (XCB), and the rotary core barrel (RCB). Any of these systems is applied to maximize core recovery in the lithology being drilled. Drilling systems and their characteristics, such as drilling-related deformation, are summarized in the "Explanatory Notes" chapter of the Leg 139 *Initial Reports* volume, and various versions are found in all previous volumes.

Shipboard Scientific Procedures

Numbering of sites, holes, cores, and samples followed the standard ODP procedures. A full identification number for a sample consists of the following information: leg, site, hole, core number, core type, section number, piece number (for hard rock), and interval in centimeters measured from the top of the section. For example, a sample identification of "151-907A-10H-1, 10–12 cm" would be interpreted as representing a sample removed from the interval between 10 and 12 cm below the top of Section 1, Core 10 (H designates that this core was taken during hydraulic piston coring) of Hole 907A during Leg 151.

Cored intervals are referred to in meters below seafloor (mbsf); these are determined by subtracting the rig floor height above sea level (as determined at each site) from the drill pipe measurements from the drill floor. Note that this measurement usually differs from precision depth recorder (PDR) measurements by a few to several meters.

General core handling procedures are described in previous *Initial Reports* volumes and the Shipboard Scientists Handbook, and are summarized here. As soon as cores arrived on deck, core catcher samples were taken for preliminary biostratigraphic analysis, and gas void samples were taken with a vacutainer for immediate analysis as part of the shipboard safety and pollution prevention program. When the core was cut into sections, whole round samples were taken for shipboard interstitial water examinations and, from some cores, for shore-based consolidation tests. In addition, headspace gas samples were immediately scraped from the ends of cut sections and sealed in glass vials for light hydrocarbon analysis.

After whole-round sections were run through the multi-sensor track (MST; see "Physical Properties" section, this chapter) and thermal conductivity measurements were performed, the cores were split into working and archive halves. Cores were split from the bottom to top, so investigators should be aware that older material could have been transported upward on the split face of each section. The working half of each core was sampled for both shipboard and shore-based laboratory studies; the archive half was described visually and by means of smear slides and thin sections taken from the working half. Most archive sections were run through the cryogenic magnetometer. The archive half was then photographed with both black-and-white and color film, a whole core at a time, and close-up photographs (black-and-white) were taken of particular features for illustrations in the summary of each site, as requested by individual scientists.

Both halves of the core were then put into labeled plastic tubes, sealed, and transferred to cold storage space aboard the drilling vessel. At the end of the leg, the cores were transferred from the ship into refrigerated trucks and to cold storage at the East Coast Repository of the Ocean Drilling Program, at the Lamont-Doherty Earth Observatory, Columbia University, New York. In spring 1994, the cores were transferred to the Bremen Core Repository at Bremen University, Federal Republic of Germany.

[1] Myhre, A.M., Thiede, J., Firth, J.V., et al., 1995. *Proc. ODP, Init. Repts.*, 151: College Station, TX (Ocean Drilling Program).

[2] Shipboard Scientific Party is as given in the list of participants preceding the Table of Contents.

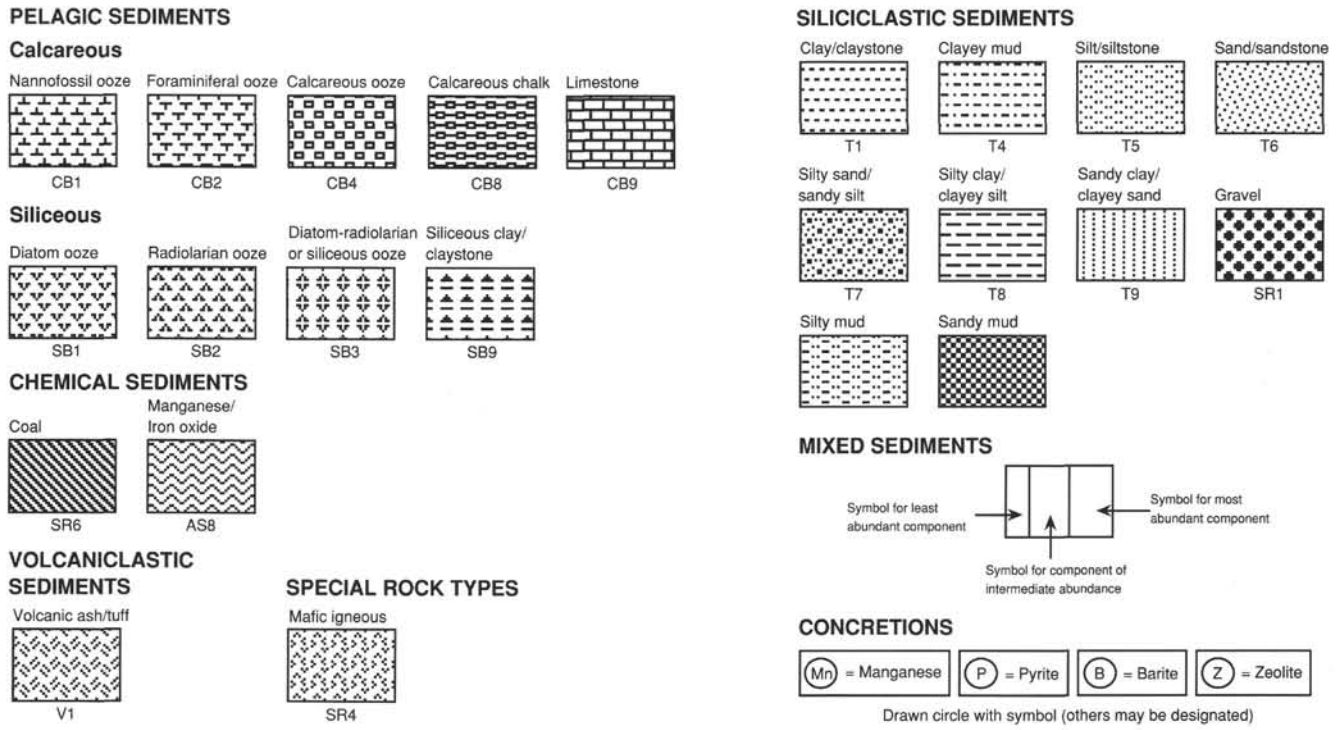

Figure 1. Key to symbols used in the graphic lithology column on the core description forms.

CORE DESCRIPTIONS

Visual Core Descriptions and the Barrel Sheet Program "VCD"

Sedimentologists aboard Leg 151 were responsible for visual core descriptions, smear-slide analyses, and thin-section descriptions of all cored sediment. Information recorded manually section by section on VCD sheets was condensed and entered into the "VCD" program, producing a graphical summary sheet. The following is a summary of the Leg 151 use of the "VCD" program.

The lithology of the recovered material was represented on the computer-generated core description forms by symbols representing up to three components in the column titled "Graphic Lithology" (Fig. 1). Where an interval of sediment or sedimentary rock was a mixture of lithological components, the constituent categories were separated by a solid vertical line, with each category represented by its own symbol. Constituents accounting for <10% of the sediment in a given lithology (or others remaining after the representation of the three most abundant lithologies) were not shown in the graphic lithology column, but were listed in the "Lithologic Description" section of the core description form. In intervals of thinly interbedded sediments comprising two or more lithologies of different compositions, the constituent categories were separated by a dashed vertical line. Because of the limited scale of the core summaries, the graphic lithology column usually shows only the composition of layers or intervals exceeding 20 cm in thickness. In some sections, layers as thin as 10 cm are shown, if they are thought to be sufficiently important.

The chronostratigraphic unit, as recognized on the basis of paleontological and paleomagnetic criteria was recorded in the "Age" column on the core summaries. Boundaries between assigned ages were indicated as follows:

1. Sharp boundary: straight line;
2. Unconformity or hiatus: line with + signs above it;
3. Uncertain: line with question marks.

The "Structure" column was used to indicate a variety of features modifying the sediment, such as primary sedimentary structures, soft-sediment modification features, structural features, and diagenetic features (Fig. 2). For Leg 151, the shipboard sedimentologists decided to use the color-banding symbols to indicate both color banding and interbedded lithologies, because the latter was invariably accompanied by color changes. The following definitions were adopted from Blatt et al. (1980, p.128):

Thick bedding/color banding >30 cm
Medium bedding/color banding 10–30 cm
Thin bedding/color banding <10 cm

The following scale was used for describing bioturbation as measured by the percentage of burrow features:

1%–30% bioturbation = slight bioturbation
30%–60% bioturbation = moderate bioturbation
60%–90% bioturbation = heavy bioturbation.

Interpretation of homogeneous sediment is difficult as it lacks any criteria by which to classify it. Leg 151 sedimentologists recognized that homogeneous sediment may be the product of deposition of material of homogeneous color and grain size resulting in sediment with no observable lamination or color change, or the product of total mixing by the action of bioturbating organisms.

Deformation and disturbances of sediment that clearly resulted from the coring process were illustrated in the "Drilling Disturbances" column. Blank regions indicate the absence of drilling disturbance. The degree of drilling disturbance was described for soft and firm sediments using the following categories:

1. Slightly deformed: bedding contacts were slightly bent;
2. Moderately deformed: bedding contacts were extremely bowed;

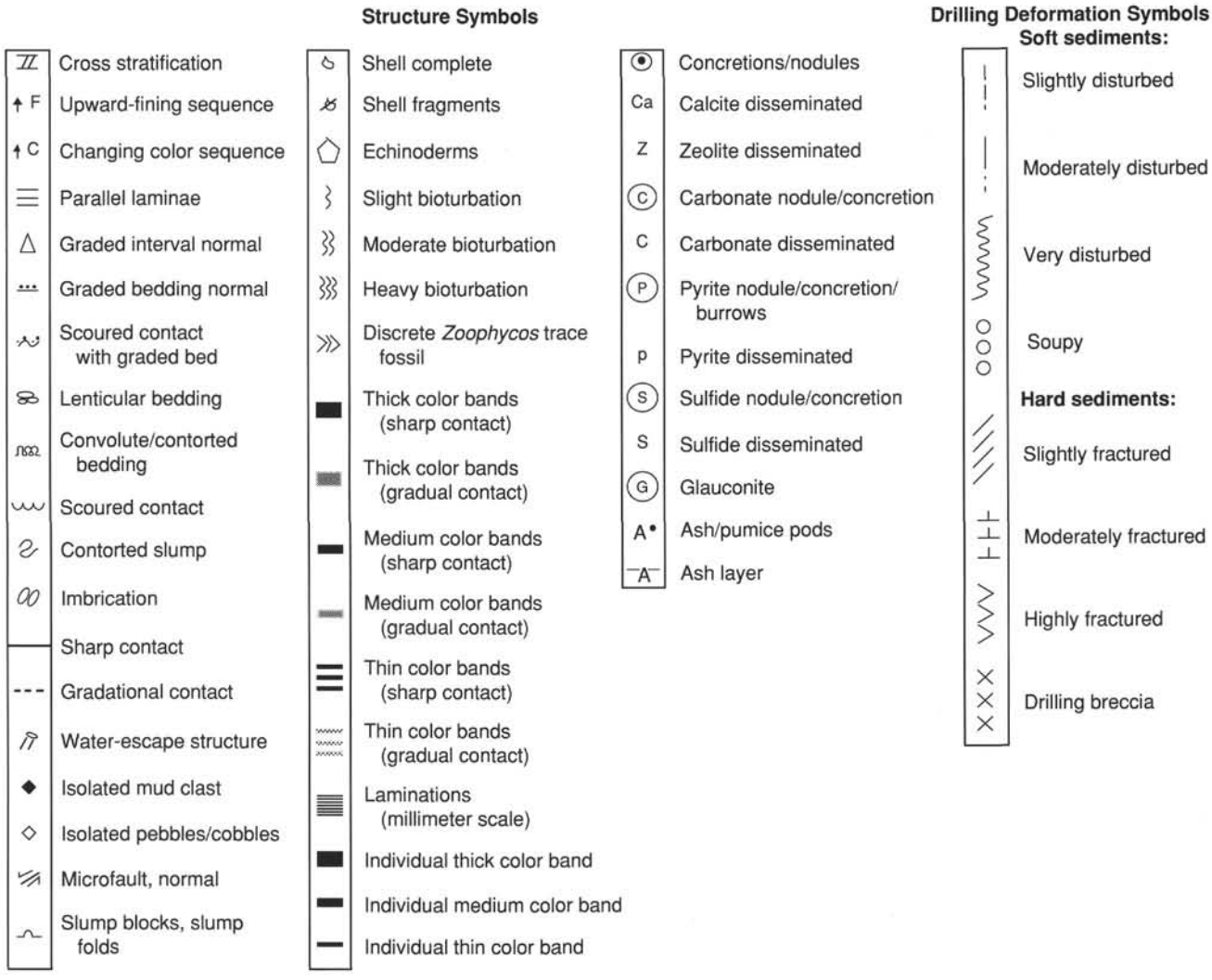

Figure 2. Symbols used for drilling disturbance and sedimentary structure on core description forms.

3. Highly deformed: bedding was completely disturbed, in some places showed symmetrical diapir-like or flow structures;
4. Soupy: intervals were water-saturated and had lost all aspects of original bedding.

The degree of fracturing in indurated sediments was described using the following categories:

1. Slightly fractured: core pieces were in place and contained little drilling slurry or breccia;
2. Moderately fragmented: core pieces were in place or partly displaced, but the original orientation was preserved or recognizable (drilling slurry may surround fragments);
3. Highly fragmented: pieces were from the cored interval and probably in the correct stratigraphic sequence (although they may not represent the entire section), but the original orientation was completely lost;
4. Drilling breccia: core pieces lost their original orientation and stratigraphic position and may have been mixed with drilling slurry.

The hue and chroma attributes of color were recorded in the "Color" column and were determined using Munsell Soil Color Charts (1971).

The location of all samples taken from each core for shipboard analysis was indicated in the "Samples" column on the core description form, as follows:

D: XRD sample
I: interstitial-water sample
M: micropaleontology sample
P: physical-properties sample
S: smear slide
T: thin section

A figure summarizing key data from smear slides appears in each site chapter, and all data derived from smear-slide and thin-section analyses appear in the "Smear Slides" and "Thin Sections" sections, this volume. Included in the "Thin Sections"section is information on the sample location, whether the sample represents a dominant ("D") or a minor ("M") lithology in the core, and the estimated percentages of sand-, silt-, and clay-size material, together with all identified components. At least one sample per core was analyzed for $CaCO_3$ percentage and total organic carbon (see "Organic Geochemistry" section, this chapter). These data are presented in the "Organic Geochemistry" section for each site.

The lithologic description that appears on each core description form consists of three parts:

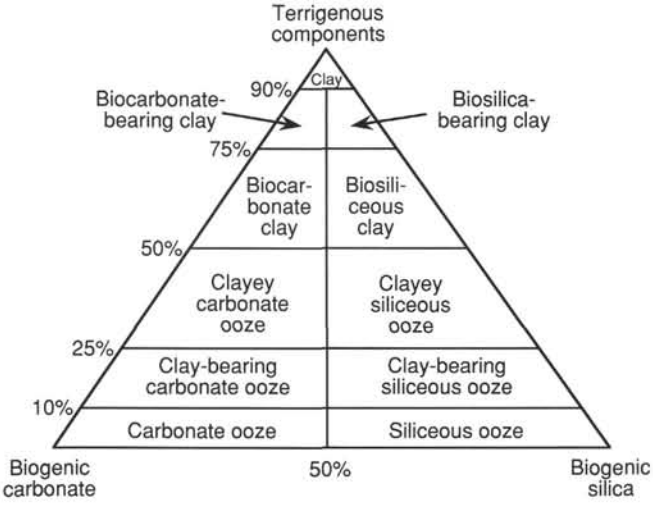

Figure 3. Compositional classification for biogenic and siliciclastic marine sediments.

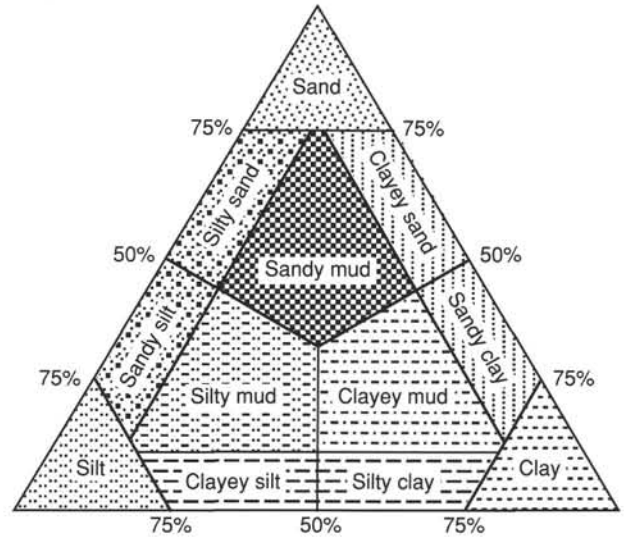

Figure 4. Lithologic classification scheme used during Leg 151 when sediments consist of >75% siliciclastic material. When the sediment consists of 50%–75% siliciclastic material, this classification scheme is used and is preceded by a modifier that describes the nonsiliciclastic component. The general term "mud" may be replaced by more specific names, such as sand, silt, clay, or gravel.

1. A heading that lists all the major sediment lithologies observed in the core;
2. A heading for minor lithologies;
3. A more detailed description of these sediments, including features such as color, composition (determined from the analysis of smear slides), sedimentary structures, or other notable characteristics. Descriptions and locations of thin, interbedded, or minor lithologies that could not be depicted in the graphic lithology column were included in the text.

SEDIMENT CLASSIFICATION

Introduction

Leg 151 sediment classification is based on smear-slide analysis and visual core descriptions. Sedimentologists chose to follow a modified version of the ODP Leg 105 sediment classification (Shipboard Scientific Party, 1987). This descriptive classification is well suited to describing glacial-marine sediment in that it distinguishes several categories of siliciclastic (gravel, sand, silt, clay) mixtures. The Leg 151 classification shown in Figure 3 is a simplification of Leg 105's classification in their "Explanatory Notes" (Shipboard Scientific Party, 1987, fig. 7).

Major sediment types are distinguished on the basis of the dominant component (>50%), which provides the principal lithological name (e.g., diatom ooze, silty sand). When a component makes up 25%–50% of the sediment, it is mentioned as a major modifier preceding the principal name (e.g., diatomaceous clay, nannofossil silty sand). Minor constituents (10%–25%) are included using the term "-bearing" (e.g., diatom-bearing clay; nannofossil-bearing silty sand). The sediment modifiers are ordered so that the minor modifier(s) precede the major modifier(s).

Specific nomenclature for each major compositional group is given below.

Siliciclastic Sediments

The siliciclastic category includes sediments having >50% siliciclastic sediments. These sediments are classified on the basis of size. Specific size designations are shown in Figure 4. This classification differs from that of Leg 105 in that sediments having >75% of a single component are given that name (e.g., 23% silt, 77% sand = sand). When the coarse fraction contains gravel, classification follows Figure 5 (e.g., 40% gravel, 30% sand, 25% silt, 5% clay = gravelly silty mud). Sediments containing >10% gravel are described using Figures 4 and 5.

When the biogenic component is between 25% and 50%, a biogenic modifier is used as shown in Figure 3. In this case, the size designation for the siliciclastic sediments is based on the siliciclastic component only (e.g., 40% nannofossils, 25% silt, 35% clay = nannofossil silty clay). When both siliceous and carbonate biogenic particles are present, and one type of biogenic particle is more abundant than the other (e.g., silica composed of radiolarians, diatoms, and sponge spicules), the entire fraction is treated as a single entity (e.g., 10% radiolarians, 15% diatoms, 20% nannofossils, 25% silt, 30% clay = nannofossil siliceous silty clay), showing the importance of that type of biogenic particles (e.g., biosilica) rather than the individual components.

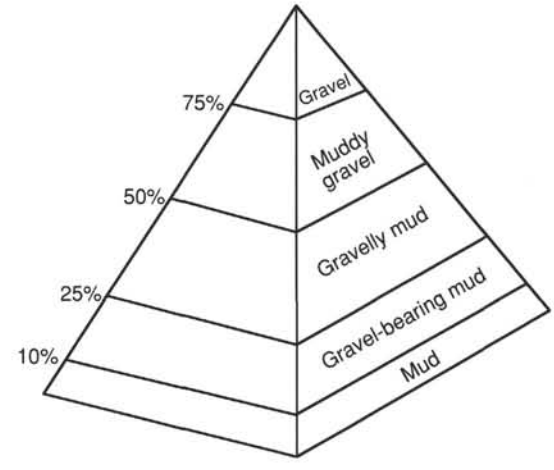

Figure 5. Classification scheme used when >10% gravel is present. Base of the tetrahedron is the classification for siliciclastic sediments (see Fig. 4).

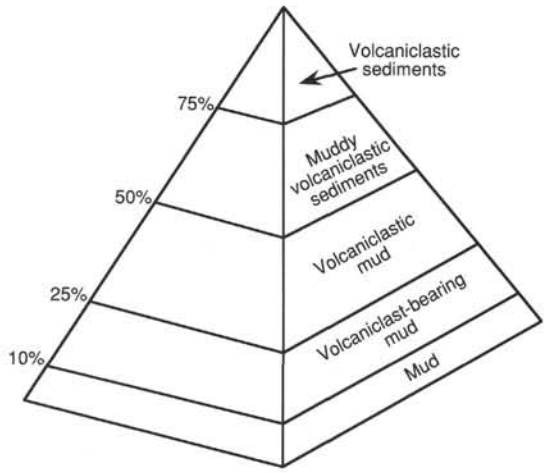

Figure 6. Classification scheme used when >10% volcaniclastic sediment is present. Base of the tetrahedron is the classification for siliciclastic sediments (see Fig. 4).

Biogenic Sediments

When the biogenic component exceeds 50%, the sediment is an ooze (or harder equivalent), following Figure 3. As with the biogenic modifiers for the siliciclastic components, the designation as siliceous or carbonate depends upon grouping all of the biogenic components with that composition, and the siliciclastic size fraction is based only on the siliciclastic component (e.g., 10% silt, 20% clay, 25% foraminifers, 15% nannofossils, 30% radiolarians = silty-clayey radiolarian carbonate ooze).

When the siliciclastic component is between 10% and 25%, it is followed by the word "-bearing." If the siliciclastic component is <10%, it is not included in the description.

Volcaniclastic Sediments

Volcaniclastic sediments are classified on the basis of their relative abundance as shown in Figure 6. The remainder of the classification follows that used during Leg 105 (Shipboard Scientific Party, 1987). Most of the volcaniclastic sediment recovered during Leg 151 was ash (pyroclastic particles <2 mm in size), and that is the term most commonly employed.

Induration

These terms follow standard ODP nomenclature (Mazzullo et al., 1988) and that used during Leg 105 (Shipboard Scientific Party, 1987).

BIOSTRATIGRAPHY

Biostratigraphy and Time Scale

Preliminary age assignments determined during ODP Leg 151 are based on biostratigraphic analyses of siliceous, calcareous, and organic-walled microfossils. Siliceous biostratigraphy includes analyses of diatoms, silicoflagellates, and radiolarians. Calcareous groups analyzed include planktonic and benthic foraminifers, calcareous nannofossils and *Bolboforma*. The organic-walled group includes dinoflagellates. Age assignments were primarily made on core-catcher samples. Additional shipboard samples were used as needed.

Biostratigraphic ages and zonal assignments established for the various fossil groups studied during Leg 151 are correlated to the geomagnetic polarity time scale established during the cruise, when possible, to determine sedimentation rates and identify hiatuses. Magnetostratigraphy of Leg 151 was correlated to numerical ages based on the chronostratigraphic time scale of Cande and Kent (1992) (see "Paleomagnetics" section, this chapter). Most published biostratigraphic zonations rely on correlation to the Berggren et al. (1985) time scale and earlier chronostratigraphic schemes.

During shipboard study, biostratigraphic assignments from Leg 151 were based on previously established biostratigraphic zonations for the Norwegian Sea, North Atlantic Ocean, and elsewhere, where possible. However, difficulties such as variable preservation, low abundance, endemism, and possible diachrony have limited the ability to correlate Leg 151 fossil assemblages to biostratigraphic zones defined from lower latitudes.

Diatoms

A new diatom biostratigraphic zonation will be proposed postcruise for the Norwegian-Greenland Sea and the "Arctic Gateway" based on material from Leg 151. The new zonation will be built on previous diatom biostratigraphic studies in the Norwegian Sea, notably those of Schrader and Fenner (1976) and Dzinoridze et al. (1978). The North Atlantic zonation of Baldauf (1984, 1987) and North Pacific zonations (Koizumi, 1973; Barron, 1980, 1985) provide useful comparisons. Because certain taxa are bipolar, the Antarctic diatom zonation of Harwood and Maruyama (1992) proved a useful reference, although the extent of interpolar diachrony is unknown.

Figure 7 shows the correlation of upper Oligocene to Holocene Norwegian Sea, North Atlantic, and North Pacific diatom zonations, according to Baldauf (1984), with the magnetic polarity time scale of DSDP Leg 81 (after Baldauf, 1984). Quantitative diatom biostratigraphic studies of Bodén (1992) from Leg 104 in the Norwegian Sea provide chronostratigraphic control for certain upper Neogene diatom datums, though absolute dating of middle to upper Miocene sections of Leg 104 was problematic. Bodén (1992) did not propose biozones for ODP Leg 104 material.

Smear slides were prepared from all core catchers and many cores during the cruise. Diatom abundance was determined based on smear-slide evaluation (at 400× magnification) using the following guide:

A (abundant) = >6 diatoms per field of view;
C (common) = 1–5 diatoms per each field of view;
F (few) = 1–4 diatoms per 5 fields of view;
R (rare) = 1–10 diatoms per horizontal traverse (54 fields of view);
T (trace) = <5 whole diatoms per slide, fragments present;
B (barren) = no identifiable diatoms or diatom fragments.

If any diatom debris were noted in smear slides, samples were prepared for biostratigraphic analyses as follows: 1–2 cc of sediment was treated with hydrochloric acid (when carbonate was present) and hydrogen peroxide until disaggregated, and washed by repeated centrifuging (2000 rpm for 3 min). Qualitative strewn slides of the cleaned samples were prepared from a subsample drawn by micropipet, and mounted on 22- by 40-mm cover glass using Norland Optical Adhesive. Certain samples, notably those with abundant clay and rare diatoms, were washed using a 20-μ mesh sieve. This method biases the assemblage toward larger diatoms, but greatly improves the chances of biostratigraphically dating diatom-poor sediments. All slides were examined using 40× (dry), 63× (oil), and 100× (oil) objectives.

Qualitative estimates of abundance of individual diatom taxa are based on the number of specimens observed per field of view using the 63× objective, and are recorded as follows:

A (abundant) = 2 or more specimens per field of view;

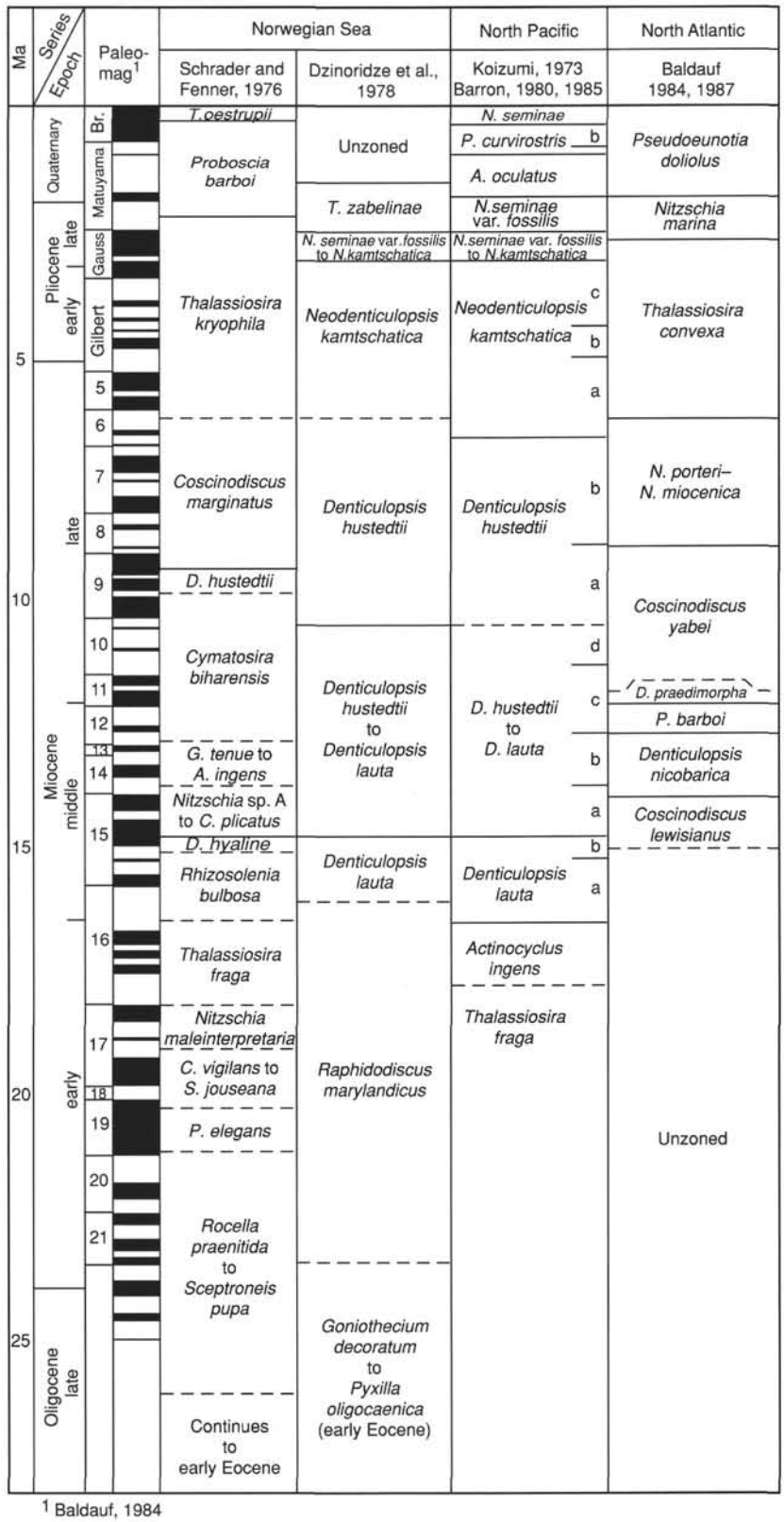

Figure 7. Upper Oligocene to Holocene diatom biostratigraphic zonations for the North Atlantic Ocean, Norwegian-Greenland Sea, and North Pacific Ocean, as compiled by Baldauf (1984). Chronostratigraphic calibration is to the magnetostratigraphic time scale of DSDP Leg 81.

C (common) = 1–5 specimens per 5 fields of view;
F (few) = 2–10 specimens per horizontal traverse;
R (rare) = ~1 specimen per horizontal traverse;
T (trace) = single specimen or fragment observed.

Estimation of preservation of diatoms was determined qualitatively and recorded as follows:

G (good) = both finely silicified and heavily robust forms present, no significant alteration of the frustules observed, other than minor fragmentation;
M (moderate) = some finely silicified forms present, some alteration present;
P (poor) = finely silicified forms rare or absent, assemblage dominated by robust forms and fragments.

Silicoflagellates

Slides prepared for diatoms also were analyzed for biostratigraphically significant silicoflagellates. Preliminary biostratigraphic analysis of silicoflagellates in Leg 151 sediments followed studies by Perch-Nielsen (1985b) and Norwegian-Greenland Sea studies by Martini and Müller (1976), Bukry (1976), Dzinoridze et al. (1978) from DSDP Leg 38, and Ciesielski et al. (1989) and Locker and Martini (1989) from ODP Leg 104. No silicoflagellate zonation was used during Leg 151.

Radiolarians

Ages of Neogene radiolarian faunas from the Norwegian and Greenland Seas are determined from zonations established for this area by Bjørklund (1976) and Goll and Bjørklund (1989). Correlation of radiolarian events by Goll and Bjørklund (1989) to the magnetic polarity time scale obtained on Leg 104 is problematic for the Miocene section, and is being reevaluated based on data collected during this cruise. Biostratigraphic zonations for the Paleogene of high northern latitudes are in the earliest stage of development and have been developed only partially for the Norwegian and Greenland Seas. Ages for those radiolarians herein are based on comparison with material from DSDP Leg 38 in the Norwegian-Greenland Sea (Bjørklund, 1976; Dzinoridze et al., 1978) and studies from the North Atlantic and Labrador Sea (Westberg-Smith and Riedel, 1984; Lazarus and Pallant, 1989). Little has been published on the taxonomy of radiolarians from the Arctic Ocean proper (e.g., Hülsemann, 1963; Kruglikova, 1989), and no biostratigraphic zonations exist for this region. Age assignments are based on known biostratigraphic ranges of non-endemic species recovered from core material.

Samples were placed in one of the following solutions to break down sediment and remove clays: (1) a mixture of water and Calgon (approximately 2 teaspoons per 500 ml of water); (2) a 15% hydrogen peroxide solution; or (3) a 80:20 solution of 30% hydrogen peroxide and water mixed with 10% sodium pyrophosphate. Samples partially disaggregated after soaking for 5 to 10 min without heat in one of the above solutions. After being cleaned, samples were sieved at 63 µm to remove clays and small diatoms. Strewn slides were prepared from the residues using Norland Optical Adhesive or Permount mounting medium.

Semi-quantitative estimates of total radiolarian abundances are based on traverses across strewn slides prepared from processed samples. Abundances are recorded as follows:

A (abundant) = >100 specimens per slide traverse;
C (common) = 50–100 specimens per traverse;
F (few) = 10–50 specimens per traverse;
R (rare) = <10 specimens per traverse.

Preservation is recorded as follows:

E (excellent) = nearly pristine, complete skeletons, lacking any indication of dissolution, recrystallization or mechanical breakage;
G (good) = majority of the specimens complete; minor dissolution, recrystallization and/or breakage;
M (moderate) = dissolution, small amount of recrystallization or breakage of specimens;
P (poor) = extensive dissolution, recrystallization or breakage of specimens.

Calcareous Nannofossils

The zonal scheme established by Martini (1971) was employed during Leg 151. Numerous upper Pliocene to Quaternary biostratigraphic events recognized by Takayama and Sato (1987) and Sato et al. (1991) were used. These events were found in the uppermost Cenozoic sediments of the North Atlantic Ocean and are not in Martini's zonal boundary definitions.

Nannofossil slides were prepared from unprocessed material. Preservation of calcareous nannofossils in smear slides was recorded using the following description:

G (good) = little or no evidence of dissolution;
M (moderate) = minor dissolution or crystal overgrowth observed;
P (poor) = strong dissolution or crystal overgrowth, many specimens unidentifiable.

Nannofossil abundance was recorded as follows:

A (abundant) = >1 specimen per field of view;
C (common) = 1 specimen per 2 to 10 fields of view;
F (few) = 1 specimen per 11 to 100 fields of view;
R (rare) = 1 specimen per 101 to 1000 fields of view;
B (barren).

Foraminifers

The biostratigraphic value of the "P" (Paleogene) and "N" (Neogene) zones of Blow (1979) established for low latitudes has limited value in middle and high latitudes because temperature is one of the controlling factors in the distribution of planktonic foraminifers in the oceans. The taxa can be roughly divided into warm-water assemblages and cold-water forms. The area under investigation falls, according to the major world distribution of Holocene planktonic foraminifers, in the Subarctic and Arctic zones. In the Subarctic Zone eight species of planktonic foraminifers occur. In the Arctic Zone the total number of species decreases to five (Bé and Tolderlund, 1971). In the Neogene sediments of the Vøring Plateau, the direction of coiling in different species of *Neogloboquadrina* may be used to separate zones (Spiegler and Jansen, 1989). Shore-based studies of oxygen isotopes may aid in the establishment of a planktonic foraminifer-based stratigraphy for the higher latitudes.

The preparation methods used to obtain planktonic and benthic foraminifers included disaggregation and wet sieving over a 63-µm sieve. The sediments were dried and the foraminifers were separated under the binocular microscope. Several different methods were used for disaggregation, including ultrasonic treatment, hot Calgon solution, and hydrogen peroxide for consolidated sediments. A 20-cc sample was measured by displacement for use in calculating the abundances of the foraminifers. In the range charts the abundances are categorized as:

A (abundant) = more than 250 specimens in 20 cc;
C (common) = 25–250 specimens;
F (few) = 5–25 specimens;

R (rare) = 1–5 specimens;
B (barren).

Preservation is categorized as G (good), M (moderate), and P (poor). Planktonic/benthic ratios were determined to reveal environmental conditions and dissolution patterns.

Bolboforma

The *Bolboforma* zonation may have the potential to become a useful supplementary biostratigraphic tool in Cenozoic middle and higher latitude calcareous sediments. *Bolboforma* has been found in numerous DSDP and ODP sites. Thirteen zones were established for the middle Eocene to upper Pliocene (Spiegler and Daniels, 1991). Seven of these zones were established in the Norwegian Sea (Qvale and Spiegler, 1989). Cenozoic *Bolboforma* zonations calibrated to calcareous nannofossil stratigraphy and magnetostratigraphy have been published for North Atlantic sites (Spiegler and Müller, 1992) and on subantarctic Atlantic ODP Leg 114 (Spiegler, 1991). A revision of the upper/middle Miocene boundary on the Vøring Plateau (ODP Leg 104), based on correlation of calcareous nannofossils and *Bolboforma*, is given by Müller and Spiegler (1993). *Bolboforma* lived in temperate to cold conditions and is indicative of subarctic/subantarctic to transitional water masses.

The preparation methods used to obtain *Bolboforma* were the standard techniques used for foraminifers described above. The occurrences of *Bolboforma* specimens are designated as:

A (abundant) = more than 25 specimens per 20 cc;
C (common) = 11–25 specimens;
R (rare) = 1–10 specimens.

Dinoflagellates

The dinoflagellate zonations of Mudie (1989) and Manum et al. (1989) from the Norwegian Sea were followed during Leg 151. The studies of deVernal and Mudie (1989a, b), Head et al. (1989b, c), and Head and Norris (1989) from Baffin Bay and the Labrador Sea were relied upon also, along with the general biostratigraphic compilation of Powell (1992). Abundances of individual taxa were recorded as follows: Abundant = >25% of assemblage, Common = 10%–25%, Few = 2%–10%, Rare = <2%.

Samples were macerated with (1) HCl and (2) HF. When samples had little or no carbonate in them, samples were placed in a beaker with water and physically broken up and stirred with a spatula. The muddy water was sieved through a 20-µm sieve and then centrifuged. After the water was poured off, the samples underwent HF treatment, were washed and centrifuged to neutrality, and sieved again with a 20-µm sieve. Strewn mounts of the residue were made, using Norland Optical Adhesive.

PALEOMAGNETICS

Paleomagnetic studies performed aboard the *JOIDES Resolution* during Leg 151 included routine measurements of natural remanent magnetization (NRM) and of magnetic susceptibility of sedimentary, volcanic, and basement material. The measurement of magnetic remanence was generally accompanied by alternating field (AF) or thermal demagnetization to remove secondary magnetizations.

Laboratory Instruments

General

The paleomagnetic laboratory on the *JOIDES Resolution* maintained two magnetometers for measurement of magnetic remanence during Leg 151: a pass-through cryogenic superconducting rock magnetometer (SRM) manufactured by 2-G Enterprises (Model 760R) and a Molspin spinner magnetometer. The laboratory has an alternating field demagnetizer and a thermal demagnetizer (Models GSD-1 and TSD-1 by the Schonstedt Instrument Co.) capable of demagnetizing discrete specimens to 100 mT and 700°C, respectively. In addition, an in-line AF demagnetizer is included in the pass-through SRM track. This unit was upgraded during the port call before Leg 151 with a modified coil system capable of AF demagnetization to 30 mT. The coils are enclosed in a mu-metal shield that attenuates the ambient field to less than 100 nT, although the field within the AF demagnetization coils varies ±100 nT with ship's motion. The shields were AF demagnetized if the field in the demagnetizer was >100 nT. Tests on deep-sea sediment discrete samples suggest no significant parasitic anhysteretic remanent magnetization (ARM) at 30-mT demagnetization levels or below for typical samples.

The sensing coils in the SRM measure the signal over about a 20-cm interval, and the coils for each axis have slightly different response curves. The widths of the sensing regions correspond to about 200–300 cm^3 volume of cored material, which contributes to the signal at the sensors. The large volume of core material within the sensing region permits accurate determination of the remanence for weakly magnetized samples, despite the relatively high background noise related to the motion of the ship.

The pass-through SRM and its AF demagnetizer are controlled by Quick BASIC programs CRYOSECT and CRYOCUBE running on a PC-AT-compatible computer. The spinner magnetometer, used for measuring discrete samples, was interfaced with a Macintosh SE/30 with a program brought on board by David Schneider Ltd. for Leg 138.

The magnetic susceptibility of whole cores was measured with a Bartington Instruments magnetic susceptibility meter (Model MS1, adapted with a MS1/CX 80-mm whole-core sensor loop set at 0.465 kHz), mounted with the GRAPE and *P*-wave logger on the multi-sensor track (MST). The full width of the impulse response peak at half maximum is less than 5 cm. The susceptibility of discrete specimens can be measured on board with a sensor unit (type MS1B) attached to the Bartington susceptibility meter.

For Leg 151 an Analytical Services Company (ASC) model IM-10 impulse magnetizer and a Kappabridge KLY-2 (Geofyzika Brno) also were available on board. The IM-10 impulse magnetizer is for studies of the acquisition of stepwise and saturation isothermal remanence magnetization (IRM) in discrete samples. This unit can apply pulsed fields from 20 to 1,200 mT. The Kappabridge is a semi-automatic autobalance inductivity bridge with a high sensitivity (4×10^{-8} SI units) and an accuracy of ±0.1% within one measuring range. The induced magnetization of the specimens is determined in 15 positions in a 300 A/m field, and the susceptibility tensor (K_{ij}) is calculated from the measurements. The principal magnitudes and directions of K_{ij} are obtained by the diagonalization of the tensor; the principal directions are given by the eigenvectors, and the principal magnitudes by the eigenvalues.

Cross Calibration of Cryogenic Magnetometer Axes

The mutual calibration of the three squid sensors was checked by rotating a calibration sample (a small piece of magnetic recording tape mounted in a paleomagnetic sample box) into the *x*, *y*, and *z* directions defined by the discrete sample holder resting in the core track and then reading the digital voltmeter outputs on the SRM modules. Magnetic moments were calculated using the emu/phi constants supplied by 2G with the instrument (*x*: 0.000174, *y*: 0.0001646, *z*: 0.0001215). These are the constants imbedded in the CRYOSECT and CRYOCUBE programs of Leg 151. The three axes appeared to be cross calibrated within 1%. Cross calibration of the axis responses was accomplished through digitalized response functions embedded in the CRYOSECT software.

Determination of Coil Constants

To effectively demagnetize cores without directional bias, the three (x, y, z) coil sets must each produce an equal AF demagnetization effect. The installation of new degaussing coils during port call necessitated a calibration of the coil constants. With the 2G AF controller generating its maximum current, the AF field induction was measured perpendicular to the axis of each coil set with the ship's Walker MG50P Hall Effect gaussmeter. This instrument showed good calibration (±1%–2%) with a Hall Effect Probe that W. Goree of 2G, Inc. brought on board in port. The peak fields produced at a thumbwheel setting of 1999 (x = 474 gauss, y = 461 gauss, z = 1283 gauss in demagnetizer coordinates with a reproducibility of ±2 gauss) were used to calculate the coil constants that the CRYOSECT and CRYOCUBE programs used, and differ from previous cruises.

Field Trapped in the Superconducting Shield

After the magnetometer liquid helium dewer was replenished in St. John's (filled to 92% of capacity), it was determined that the trapped magnetic field was excessive. Using the shield heaters, the trapped field was reduced to 32 nT (mostly in the y direction) at the center of the measurement region. Sharp field gradients remained in the sample access and produced higher fields in the measurement region (up to 70 nT ± 10 cm from the center of the squid response).

Holder Magnetization and Sensitivity of Measurements

The core handling boat had a measurable remanence (maximum ~5×10^{-9} Am^2), which was unremovable but very stable after AF demagnetizing to 30 mT and cleansing with alcohol. Subtracting the stable boat remanence from each core section measurement yielded a nominal noise level of ~10^{-5} Am^{-1}, which is 10–100 times less intense than magnetizations measured in sediments from the North Atlantic Ocean (e.g., Bleil, 1989). This nominal noise level was significantly degraded by the tendency of the cryogenic magnetometer to record false "flux jumps" on occasion. Several remeasurements of core sections were sometimes necessary during these episodes of spurious flux jumps to keep the noise level below 10% of the core magnetization.

Paleomagnetic Measurements

Remanent Magnetization Measurements

Remanence measurements of sediments and rocks were performed by passing continuous archive half-core sections through the SRM. The ODP core orientation scheme arbitrarily designates the positive X-axis direction as the horizontal (in situ) line radiating from the center of the core through the space between a double line scribed lengthwise on the working half of each core liner. Based on the quality of the pass-through record and AF demagnetization of discrete "pilot" samples in the GSD-1 AF demagnetizer, AF demagnetization levels were chosen that best isolated a characteristic magnetization and magnetostratigraphic record. Discrete samples in soft sediment were taken using oriented standard plastic boxes (6 cm^3). To reduce the deformation of the sediment, the core was cut using a thin stainless spatula before pressing the plastic sampling boxes into the sediment. Minicores (10 cm^3) were drilled from lithified sedimentary rocks and igneous rocks using a water-cooled nonmagnetic drill bit attached to a standard drill press.

Low-field Susceptibility

Whole-core susceptibility measurements are relatively rapid to make, are nondestructive, and provide an indication of the amount of magnetizable material in the sediment, including ferrimagnetic and paramagnetic constituents. Whole-core volume magnetic susceptibility was measured on the automated multi-sensor track (MST). Measurements were performed at the low sensitivity range (1.0) and in the cgs mode usually at a 5-cm spacing. The susceptibility response is a function of the mineralogy as well as the shape and volume of the magnetic particles within the rocks. Because magnetic susceptibility is slightly temperature-dependent, the cores were permitted to equilibrate thermally before analysis. The general trend of the susceptibility data curve was used to characterize the magnetic material contained within the cored sediments as well as subtle environmental and geologic changes within the sediments.

Core Orientation

Core orientation of the advanced hydraulic piston cores (APC) was attempted on a case-by-case basis by using a Tensor Multishot tool, which is rigidly mounted onto a nonmagnetic sinker bar. At the bottom of the hole the core barrel was allowed to rest for sufficient time (2–8 min) to permit an accurate reading of the magnetic and gravity sensors. The Tensor Multishot tool consists of three mutually perpendicular magnetic sensors and two perpendicular gravity sensors. The information from both sets of sensors allows measurement of the azimuth and dip of the hole as well as the azimuth of the APC core double orientation line. Due to the high inclination of the geomagnetic field at the drill sites (>80°), orientation data were judged to be of little value to the interpretation of polarity; the time necessary to orient a core was weighed against the value of the information at each site, and a decision was made whether or not to orient core.

Magnetostratigraphy

To maximize the chances for successful determination of the magnetostratigraphy and to satisfy the sampling needs of the shipboard paleomagnetists, who are also interested in high-resolution studies of geomagnetic and global environmental changes, an effort was made to take most of the shipboard samples from the A holes at each site, leaving the initial post-cruise sampling of the B and C holes for further paleomagnetic studies. A subset of the shipboard samples was AF demagnetized in the GSD-1 to evaluate the effectiveness of the pass-through demagnetization routine in isolating a characteristic magnetization.

Magnetozones were defined on the basis of at least two successive depths of same polarity, and the boundary between two successive magnetozones was defined by the depth at which the interpolated inclination record crossed zero inclination. The ultimate time resolution of the paleomagnetic record depends on sediment accumulation rates and the resolution of the pass-through measurements, which are limited to approximately 10 cm by the coil geometry. For shipboard measurements the measurement interval was generally 10 cm.

Where AF demagnetization isolates a consistent record of geomagnetic polarity, we offer an interpretation of the magnetic polarity stratigraphy of the recovered core in the site chapters. The Geomagnetic Polarity Time Scale (GPTS) of Cande and Kent (1992) was used to assign numerical ages to magnetozone boundaries. In each chapter we attempt to reconcile the magnetostratigraphy with biostratigraphic interpretations.

If short geomagnetic features are observed in the magnetic record, they may be useful stratigraphic markers for stratigraphic or temporal correlations. For the upper part of the time scale (roughly Pliocene-Pleistocene), we use the traditional proper or place names to refer to various chrons and subchrons (Mankinen and Dalrymple, 1979). For older sediments we follow the convention of using correlative anomaly numbers prefaced by the letter "C." Normal polarity subchrons are referred to by adding suffixes ("1n," "2n"), which increase with age. The reversal boundaries themselves are specified by the chron/subchron designation followed by the letter "o" (for onset) or "t" (for

termination). Reverse polarity chrons or subchrons are similarly named with an "r" suffix (the reverse polarity portion of a chron being older than the corresponding normal polarity).

IGNEOUS PETROLOGY

Petrographic descriptions of igneous and metamorphic core follow the format used during Leg 140 (Shipboard Scientific Party, 1992b). Core is described using visual core description (VCD) forms; the information also is entered into the HARVI database. Thin-section descriptions are recorded in the HRTHIN database. The terminology used during Leg 140 for textural analysis of igneous and metamorphic cores has been adhered to for the Leg 151 igneous and metamorphic cores with some exceptions. Descriptions of igneous contacts and lithologies are not expanded upon in separate appendixes, although descriptions of igneous and metamorphic "dropstones" are in a separate appendix. Rock names given on the VCD forms are based solely on the hand specimens, and names given with each thin-section description are based upon mineralogy and textures. In addition, volcanic rocks are classified using the criteria outlined by Williams et al. (1982, p. 96–112) and the nomenclature of Cox et al. (1979).

Methods of crushing and grinding and major element analysis by X-ray fluorescence are the same as those described by Leg 140 (Shipboard Scientific Party, 1992b). Major element analyses of reference standard BIR are presented in Table 1. Repeated analysis of reference standard BIR, analyzed along with the basalts from Leg 151, provides an estimate of precision (Table 1).

Table 1. Major element analyses of reference standard BIR analyzed as a secondary standard with basalts from Leg 151.

Sample	BIR-1B	BIR-1B	BIR-1B
SiO_2	47.60	47.60	47.60
TiO_2	0.96	0.96	0.94
Al_2O_3	15.40	15.40	15.40
Fe_2O_3*	11.40	11.30	11.40
MnO	0.17	0.17	0.17
MgO	9.67	9.58	9.64
CaO	13.30	13.10	13.20
Na_2O	1.90	1.88	1.88
K_2O	0.03	0.03	0.03
P_2O_5	0.04	0.05	0.05
Total	100.47	100.07	100.31

*Total iron as Fe_2O_3

INORGANIC GEOCHEMISTRY

Interstitial Water

Interstitial water samples were analyzed for Na, K, Mg, Ca, Cl, and SO_4 by ion chromatography; pH was measured and alkalinity determined by titration. Cl also was determined by titration as a check on ion chromatography data. NH_4 and SiO_2 were determined by spectrophotometry. Units reported are in millimoles (or micromoles) per liter. Densities are not determined, and salinities are only approximated by refractometer measurements. As a consequence, conversion to standard units (molality or molinity) is not conducted. All interstitial water analyses followed ODP standard procedures.

Sediments

Major element abundances were measured on ground, 20-cm^3 samples by X-ray fluorescence on pressed pellets following the procedure described in the "Explanatory Notes" chapter, ODP Leg 124 (Shipboard Scientific Party, 1990, p. 19–20). Although the sum of the oxides rarely equals 100% (due to the inability of the XRF to detect C and O, and thus carbonate CO_2, and the omission of S and Cl from the analysis scheme), the results are suitable for understanding variations in sediment composition. Table 2 shows the precision obtained by 40 analyses of the USGS SCo-1 (Cody Shale) standard along with accepted values (Govindaraju, 1984) for major elements in this standard.

Table 2. Analytical precision and accuracy of the shipboard XRF technique as established by 40 analyses of the composition of the USGS SCo-1 (Cody Shale) standard.

Measured concentrations oxide	Mean (wt%)	1 sigma	Coefficient of variation (%)	Accepted concentrations (Govindaraju, 1984)
SiO_2	63.04	0.19	0.30	63.39
TiO_2	0.69	0.00	0.54	0.62
Al_2O_3	13.76	0.06	0.45	13.70
Fe_2O_3*	5.78	0.03	0.57	5.22
MnO	0.05	0.00	0.00	0.05
MgO	2.73	0.01	0.42	2.76
CaO	2.66	0.01	0.32	2.64
Na_2O	0.74	0.01	1.02	0.95
K_2O	3.00	0.01	0.29	2.82
P_2O_5	0.24	0.01	2.55	0.22
Total	92.69			92.37

*Total iron as Fe_2O_3

ORGANIC GEOCHEMISTRY

The routine shipboard organic geochemistry program for Leg 151 includes: (1) analyses of hydrocarbon gases; (2) determination of inorganic carbon concentrations; (3) elemental analyses of total nitrogen, carbon, and sulfur; and (4) characterization and maturity of organic matter. All methods and instruments used during Leg 151 are described in detail by Emeis and Kvenvolden (1986) and in the "Explanatory Notes" chapter of ODP Leg 146.

Hydrocarbon Gases

For safety considerations, concentrations of methane (C_1), ethane (C_2), and propane (C_3) gases were monitored in every core, using a Carle AGC series100/Model 211. Gases were extracted using the standard ODP headspace-sampling technique (Kvenvolden and McDonald, 1986). Whenever gas voids occurred, vacutainer samples were taken as well (for comparison between vacutainer and headspace data and further details in methodology, see Stein et al., this volume).

Inorganic Carbon

Inorganic carbon was determined using a Coulometric 5011 carbon dioxide coulometer equipped with a System 140 carbonate-carbon analyzer. The percentage of carbonate was calculated from the inorganic carbon (IC) content, assuming that all carbonate occurs as calcite as follows:

$$CaCO_3 = IC \cdot 8.33$$

Elemental Analysis

Total nitrogen, carbon, and sulfur were determined using a CNS analyzer, Model NA1500 from Carlo Erba Instruments. Total organic carbon (TOC) was calculated from the difference between total carbon (TC) and inorganic carbon:

$$TOC = TC - IC$$

Organic Matter Characterization and Maturation

The Geofina Hydrocarbon Meter (GHM) and the Delsi-Nermag Rock-Eval II pyrolysis systems were used to characterize the type and maturity of the organic matter, as described by Espitalié et al. (1977). Moreover, the GHM includes gas chromatography of the hydrocarbons evolved during pyrolysis. This allows us to identify specific hydrocarbons by comparison of the retention times with those of standards.

PHYSICAL PROPERTIES

Introduction

High-resolution shipboard measurements of physical properties provide sediment parameters for characterizing geotechnical and lithologic units for downhole and cross-hole geophysical logging correlation, investigating cyclic and/or periodic events, and interpreting seismic reflection data. In addition to providing a link between lithologic and geophysical data, the goal of the physical properties program was to identify the physical signals recorded in the sediments that result from paleoceanographic change and diagenesis.

Nondestructive measurements of whole-round core sections were obtained from four sensors mounted on the multi-sensor track (MST), including a gamma-ray attenuation porosity evaluator (GRAPE), a compressional-wave core logger (PWL), a magnetic susceptibility meter, and a multichannel natural gamma spectrometer. These sensors provided high-resolution measurements of bulk density, compressional-wave velocity, magnetic susceptibility, and natural gamma activity, respectively. Thermal conductivity measurements were performed at discrete intervals in unlithified whole-round sections using a full-space needle probe method.

In unlithified sediment, measurements from the working half of the core included undrained vane shear strength and compressional-wave (*P*-wave) velocity. In the more lithified sediments, thermal conductivity was measured using a half-space needle probe method, *P*-wave velocities were determined from cut pieces of the sediments, and strength was measured using a hand-held penetrometer. Throughout the core, index properties (wet-bulk density, dry-bulk density, grain density, water content, porosity, and void ratio) were determined from discrete samples. The frequency of samples taken was typically 2/section in the upper 100 mbsf, and 1/section or less below this depth. The samples were chosen to be representative of relatively undisturbed material in the core. Some of the dried samples also were used for organic and inorganic geochemical analyses (see "Geochemistry" sections, this chapter).

Multi-sensor Track (MST)

Individual unsplit core sections were placed horizontally on the MST, which provided whole-round scans using the GRAPE, PWL, magnetic susceptibility, and natural gamma sensors.

The GRAPE provided measurements of bulk density at 1- to 2-cm intervals by comparing the attenuation of gamma rays through the cores with attenuation through aluminum and water standards (Boyce, 1976). GRAPE data are useful in correlating between holes and sites by observing peak-to-peak spacings and overall trends in the data.

The PWL transmits a 500-kHz compressional-wave pulse through the core at a repetition rate of 1 kHz using transmitting and receiving transducers that are aligned perpendicular to the core axis. The receiver detects the traveltime of the acoustic signal to an accuracy of 50 ns, which corresponds to an instrument resolution of 1.5 m/s under optimal conditions. A pair of displacement transducers monitor the separation between the compressional-wave transducers so that variations in the outside diameter of the liner do not degrade the accuracy of the velocities. Measurements were taken at 2.5-cm intervals, and weak returns having low signal strengths were removed. The GRAPE (and PWL data) were most reliable in APC cores because they had the least disturbances; in XCB cores the drilling slurry between XCB "biscuits" disturbed the core and gave lower bulk densities and unreliable velocities. The PWL often was not used because the high gas content in the cores caused high attenuation of the sonic pulse due to fracturing and cracking from gas expansion in these areas.

Bulk magnetic susceptibility measurements were made at 3-cm intervals using a Bartington magnetic susceptibility meter with an 80-mm diameter loop. The cores were exposed to a 1-Oersted alternating field as they passed through the loop. Magnetic susceptibility is reported in uncorrected cgs units.

Core gamma spectrometry measurements were performed to acquire total natural gamma counts. These counts can be used to determine elemental concentrations of ^{232}Th, ^{238}U, and ^{40}K after calibrating each spectral window to standard samples.

Thermal Conductivity

Thermal conductivity was measured using the needle probe method in full-space configuration for soft sediments (von Herzen and Maxwell, 1959) and in half-space mode for lithified sediment or hard rock (Vacquier, 1985).

Measurements were performed with a Thermcon-85 unit, and all data are reported in units of W/m·K. The estimated error in the measurements is about 5%–10%. The cold bottom-water temperatures at these sites required a 4–8 hr pre-run thermal equilibration period for each of the cores. No tests were conducted until the temperature drift was reduced to 0.04°C/min, which generally corresponded to a standard error of 2.5–2.7 × 10^{-3} W/m·K.

Thermal conductivity is calculated from the rate of heat loss in the probe while a constant heater current is flowing. The change in temperature should vary logarithmically with time as:

$$T(t) = (q/4\pi k)\ln(t) + \text{constant}, \quad (1)$$

where k is the thermal conductivity; T and t are the temperature and time, respectively; and q is the heat generated per unit length of the probe. Using Equation 1, the thermal conductivity is derived from the slope of temperature vs. the logarithm of time. Measurements of thermal conductivity using the full-space method were performed until the sediment became too lithified to insert the needle probes. After this point, the half-space mode was used where the water-saturated samples of crystalline rock were equilibrated in a water bath at room temperature before making the submerged thermal conductivity measurements.

In-situ Temperatures

Measurements of the geothermal gradient are important for calculating the stability of gas hydrates and for evaluating observed changes in the composition and concentrations of gas contained in the sediment (see "Organic Geochemistry" section, this chapter). The measured downhole temperature gradient is multiplied by the mean thermal conductivity to calculate an average heat flow. These data are based on measurements spanning several hundred meters and form an interesting comparison with existing heat-flow measurements from in-situ probes inserted a few meters into the seafloor (Crane et al., 1988).

The downhole temperatures were measured using two types of instruments, either the Adara tool or the Water Sampler Temperature Probe (WSTP). The Adara, or APC-tool, is used for measuring in-situ sediment temperatures during advanced piston coring (APC) operations. The probe and its recording electronics fit into an annular cavity inside a special coring shoe in the front end of a standard core barrel. The core barrel is deployed in the usual way and fired into the

sediments at the bottom of the borehole, thus placing the Adara probe about 9 m ahead of the drill bit and avoiding the part of the borehole influenced by drilling circulation. After the measurements are taken, the core barrel along with the sediment core is returned to the ship. The coring shoe is removed, and the temperature data are unloaded to a PC for reduction.

The WSTP is a wireline tool that is deployed through the drill string. It is landed at the bit and mechanically held in place. The temperature probe extends 1.1 m ahead of the drill bit. The bit is lowered and the WSTP is pushed down into the bottom of the borehole. If the formation is too hard for probe penetration, the probe will retract into the bit. No sediment sample is obtained using this tool. The probe is held just above seafloor to measure the temperature of the bottom water. When the probe is inserted, in-situ equilibrium temperature is estimated by fitting a theoretical decay curve to the data, which simulates the temperature change following probe penetration. If both Adara and WSTP data are collected from the same site, the temperature of the bottom water is used for intercalibration. Detailed descriptions of the techniques used for downhole temperature measurements are covered in the ODP Leg 139 "Explanatory Notes" chapter (Shipboard Scientific Party, 1992a).

Shear Strength Measurements

Sediment strength was measured at an average rate of one per core section with the Wyckham-Farrence motorized miniature vane shear device and with the Soil Test CL-700 hand-held penetrometer. The laboratory vane shear instrument can be used only in soft sediments, whereas the penetrometer is able to measure more consolidated sediments. Measurements were performed using both tools where possible to provide a comparison between the two instruments.

The vane shear is inserted perpendicular to the split-core (parallel to bedding planes) and converts a torque through a calibrated spring into a measure of the sediment's undrained shear strength (Su) given in units of kPa. The vane rotation rate was 180°/min rather than the standard 90°/min because of the set-up configuration of the instrument. The vane used for all Leg 151 measurements had a 1:1 blade ratio with a dimension of 1.27 cm. A thorough discussion on use of the Wyckham-Farrence motorized miniature vane shear device is presented by Boyce (1976).

The penetrometer estimates the unconfined compressive strength ($2 \times Su$) of the sediment (Lee, 1985) by inserting a factory calibrated spring-mounted probe ¼ inch into the sediment. The pressure of the operator's hand is converted through a calibrated spring to give a measure of soil induration. The peak value is read directly from the tool following failure of the sediments in units of kg/cm^2. Measured values range from 0.5 to 4.5 kg/cm^2, which is the maximum measurable value of this device. The conversion from unconfined strength to undrained strength requires multiplying the penetrometer readings by 98.067 kPa · cm^2/kg and then dividing by 2, which generates a range of strength measurements from 25 to 221 kPa. The penetrometer test is sensitive to the rate of penetration of the probe, which may lead to errors in measured strength from different operators. This may account for some of the scatter in the data, although core disturbance is another possibility.

Compressional-wave Velocity

In addition to the MST measurements, *P*-wave velocity was determined using two different measurement systems, depending on the degree of lithification of the sediment. Traveltimes were measured in unconsolidated sediment using a Dalhousie University/Bedford Institute of Oceanography Digital Sound Velocimeter (DSV) (Mayer et al., 1987; Courtney and Mayer, 1993). Velocity calculation is based on the accurate measurement of the traveltime of an impulsive acoustic signal traveling between a pair of piezoelectric transducers inserted in the split sediment cores. The DSV transducers were mounted with a fixed separation (approximately 7 cm). The signal used is a 2-µs square wave; the transducers have resonances at about 250 and 750 kHz. The transmitted and received signals are digitized by a Nicolet 320 digital oscilloscope and transferred to a microcomputer for processing. The DSV software selects the first arrival and calculates sediment velocity. However, often the signals were weak (because of the high attenuative properties caused by gas expansion), and then first arrivals were picked manually. Temperature of the sediments was measured with a digital thermometer probe so that corrections for in-situ temperature can be made.

When the sediments became too consolidated to insert the DSV transducers, measurements were made with the Hamilton Frame system while the split core was still in the liner. The signal path was then perpendicular to the core axis. Traveltime corrections for the core liner thickness were made. With the Hamilton Frame, a signal was transmitted and received through a pair of 500 kHz transducers mounted on a vertical press, which could be adjusted to vary the separation. Sample thickness was measured using a hand-held micrometer or directly from the velocimeter-frame lead screw. When the sediments were sufficiently consolidated, velocity measurements using the Hamilton Frame were performed on cut pieces of the sediment. The measurements were usually made along the axis of the core (in the same direction as the DSV measurements). Additionally, measurements were occasionally made perpendicular to the core axis providing a means to quantify the amount of anisotropy in the sediments. Traveltimes were corrected for the delay between the source and receiver due to the thickness of the source/receiver wareplates. This delay was found to be a function of the signal gain. Filtered seawater was used to improve the acoustic contact between the sample and the transducers. Corrections for in-situ temperature and pressure (relationships in Wyllie et al., 1956) were not made, so the velocities reported here are raw uncorrected values.

Index Properties

Index properties (water content, wet- and dry-bulk density, grain density, porosity, and void ratio) were calculated from measurements of the wet and dry weight and volume of small sediment/rock subsamples (approximately 10 cm^3). A new database software package used for calculating index properties was installed in the physical properties lab during Leg 150, and its use was continued during this leg. Values of bulk, grain, and dry density, as well as porosity and void ratio were calculated using two different methods (different sets of equations) to compare results. Data calculated using both of these methods are given in Table 14. For each sample, method "B" utilizes the "wet" or bulk sample volume measurement in the pycnometer to calculate the other values. Method "C" utilizes a dry volume measurement in calculating the other index properties; the dry volume is corrected for the weight of salt in each sample, calculated from the volume of pore fluid and assuming a constant pore fluid salinity and salt density. Method "C" is observed to produce the most consistent dry density and porosity determinations and more realistic grain densities. The dry volume includes a correction for salt assuming an interstitial pore-water salinity of 35‰ (Boyce, 1976). This correction was applied to grain density and porosity computations, as per Hamilton (1971) and Boyce (1976), but not to bulk density.

Soft sediment samples were placed in pre-calibrated aluminum containers prior to weight and volume measurements. Sample weights were determined aboard ship to a precision of ±0.01 g using a Scitech electronic balance and a specially designed statistical routine using LabView software. The individual weights were determined with a precision of 0.05 on a confidence level of 99.5%; weight was determined from *n* discrete weighings to the point where an additional weight measurement did not change the mean by greater than 5%. The mean value calculated from two determinations was used. Volumes were determined using a helium-displacement Quantachrome Penta-Pycnometer. The pycnometer measures the volume

of each sample to an approximate precision of ±0.02 cm³. Determinations were made twice and then averaged. Dry weight and volume measurements were performed after the samples were oven-dried at 110°C for 24 hr and allowed to cool in a desiccator. Bulk density (ρ) is the density of the total sample including the saline pore fluid:

$$\rho = M_t/V_t, \quad (2)$$

where V_t is the total sample volume (cm³) measured with the helium pycnometer, and M_t is the total sample mass. Grain density (ρ_g) is defined as the mass of the grains divided by the volume of the grains:

$$\rho_g = (M_d - M_s)/(V_t - V_f) = M_g/V_g, \quad (3)$$

where M_g is the mass of the grains and V_g is the volume of the grains. The salt-corrected grain density was calculated for each sample using the equation:

$$\rho_g = (M_d - M_s)/[V_d - (M_s/\rho_s)], \quad (4)$$

where M_d is the salt-corrected dry mass of sample, V_d is the dry sample volume, ρ_s is the density of salt (2.257 g/cm³), and M_s is the calculated mass of salt in the pore fluid:

$$M_s = r(M_t - M_d)/1 - r, \quad (5)$$

where r = salinity (35‰). The wet sample weight minus the dry sample weight gives the mass of the pure water (without salt). Therefore, water content (WC) as a percentage of wet weight is defined as:

$$WC_{wet} = 100 \cdot (\text{salt-corrected fluid mass})/(\text{sample bulk mass}), \quad (6)$$

whereas water content as a percentage of dry weight is defined as:

$$WC_{dry} = 100 \cdot (\text{salt-corrected fluid mass})/(\text{sample dry mass} - \text{mass of salt}). \quad (7)$$

Wet-bulk density is then defined as the ratio of weight of wet sediment to volume of wet sediment, whereas dry-bulk density is the ratio of the weight of dry sample (corrected for salt) to the volume of wet sediment. Porosity (ϕ) is defined as the ratio of the pore-fluid volume to the total volume and was determined using the quantities derived above. The following relationship was used:

$$\phi = (\rho_g - \rho)/(\rho_g - \rho_w). \quad (8)$$

Void ratio (VR) is defined as the volume of the voids (assuming fluid saturation) divided by the volume of the solids:

$$VR = (V_t - V_d)/V_d. \quad (9)$$

DOWNHOLE MEASUREMENTS

Logging Tool Strings

Downhole logs are used to directly determine physical and chemical properties of formations adjacent to the borehole. Continuous, in-situ measurements provide stratigraphic, lithologic, geophysical, and mineralogic characterization of a site. After coring at a hole is completed, a tool string (a combination of several sensors) is lowered down the hole on a 7-conductor cable, and each of the sensors continuously monitors some property of the adjacent borehole wall. Although the depths of investigation into the formation (and the resolution) are sensor-dependent, data are typically recorded at 15-cm intervals.

Four Schlumberger tool strings were used during Leg 151 (Fig. 8): the seismic stratigraphic combination, the lithoporosity combination, the geochemical combination (GLT) and Formation MicroScanner (FMS). The Lamont-Doherty Earth Observatory (LDEO) temperature tool (TLT) was attached to the base of all tool strings to obtain downhole formation/fluid temperatures. The natural gamma-ray spectrometry tool (NGT) was run as part of each tool string to correlate depths between logging runs.

The seismic stratigraphic tool string used during Leg 151 consisted of the dipole shear imager (DSI) (Fig. 9) for measuring sonic velocities, the phasor induction tool (DIT) for measuring electrical resistivity, and the NGT. The lithoporosity combination consisted of the high-temperature lithodensity tool (HLDT) for measuring formation bulk density and photoelectric effect (PEF) along with a borehole caliper measurement, the compensated neutron porosity tool (CNT) measuring formation porosity, and the NGT.

The geochemical combination consisted of the NGT, the aluminum activation clay tool (AACT), and the gamma-ray spectrometry tool (GST). This tool combination measured the relative concentrations of Si, Ca, Al, Fe, S, Ti, Gd, H, Cl, K, U, and Th.

The FMS tool string used during Leg 151 consisted of an NGT, a general purpose inclinometer tool (GPIT), and the Formation MicroScanner (FMS). The FMS and GPIT provided spatially oriented microresistivity images of the borehole wall as well as a caliper measurement of the hole width.

The data from the seismic stratigraphic, lithoporosity, and Formation MicroScanner logging combinations are recorded by Schlumberger's new MAXIS 500 digital logging unit, first deployed on Leg 149. Data from the MAXIS 500 are generated in a new data format (DLIS, Digital Log Information Standard). This is converted to LIS format (Log Information Standard) for compatibility with shipboard and shore-based logging software. MAXIS does not currently support the GLT software, which continues to be recorded on the "old" CSU (cyber service unit).

Logging Tools

A brief description of logging tools run during Leg 151 is given in the following sections. A detailed description of logging tool principles and applications is provided in Ellis (1987), Schlumberger (1989), Serra (1984), and Timur and Toksöz (1985). The specifics of each tool are summarized in Table 3, and the approximate vertical resolutions of the tools are given in Table 4.

Electrical Resistivity—Dual Induction Tool (DIT)

The DIT provides three different measurements of electrical resistivity, each with a different depth of investigation in the formation. Two induction devices (deep and medium resistivity) transmit high-frequency alternating currents through transmitter coils, creating magnetic fields that induce secondary (Foucault) currents in the formation. These ground-loop currents produce new inductive signals, proportional to the conductivity of the formation, that are measured by the receiving coils. The measured conductivities are then converted to resistivity. A third device, a spherically focused resistivity instrument, measures the current necessary to maintain a constant voltage drop across a fixed interval.

Natural Gamma-ray Spectrometry Tool (NGT)

The NGT measures the natural radioactivity of the formation by a scintillation crystal mounted inside the tool. In formations, gamma-rays are emitted by the radioactive isotope ^{40}K and by other radioactive isotopes within the U and Th decay series. Measurements are analyzed by dividing the incident gamma-ray signature into five discrete energy windows that correspond to the main spectral peaks

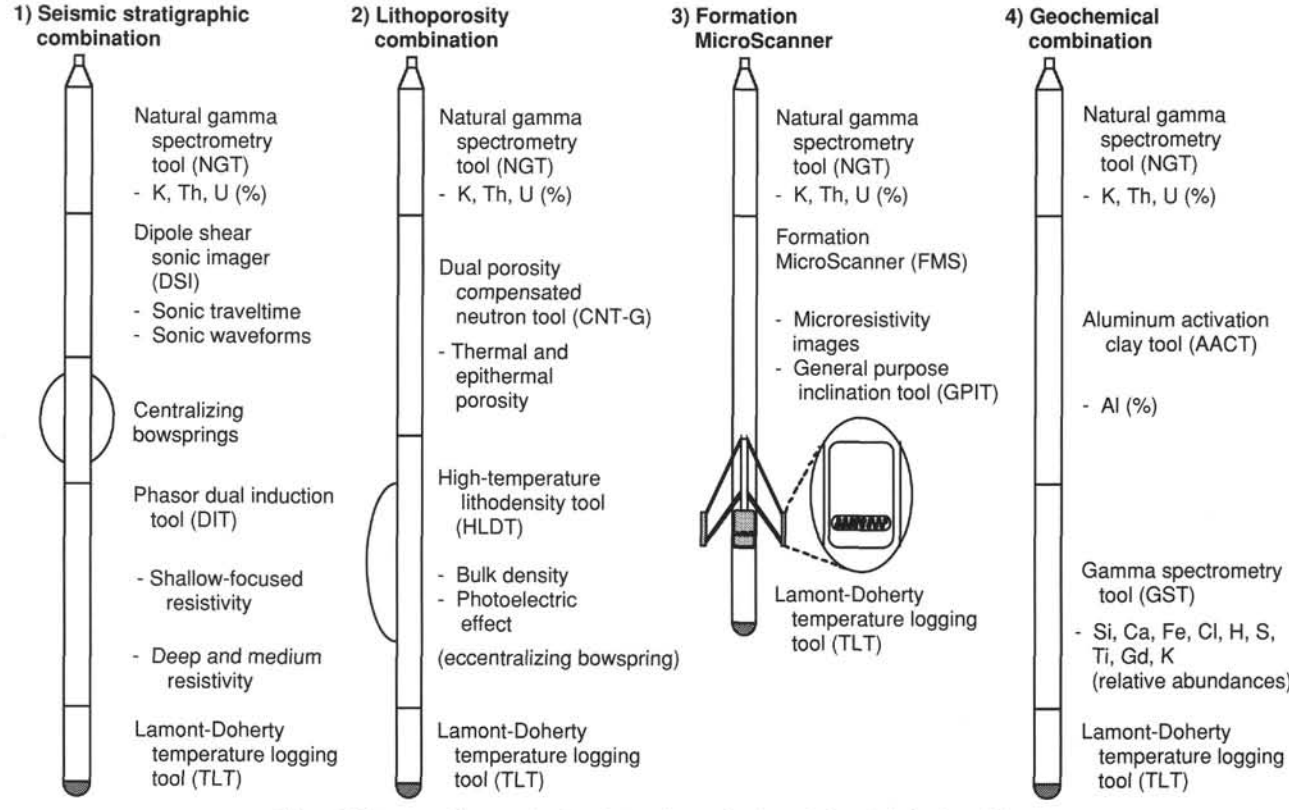

Figure 8. Summary diagram showing the logging tool strings deployed during Leg 151.

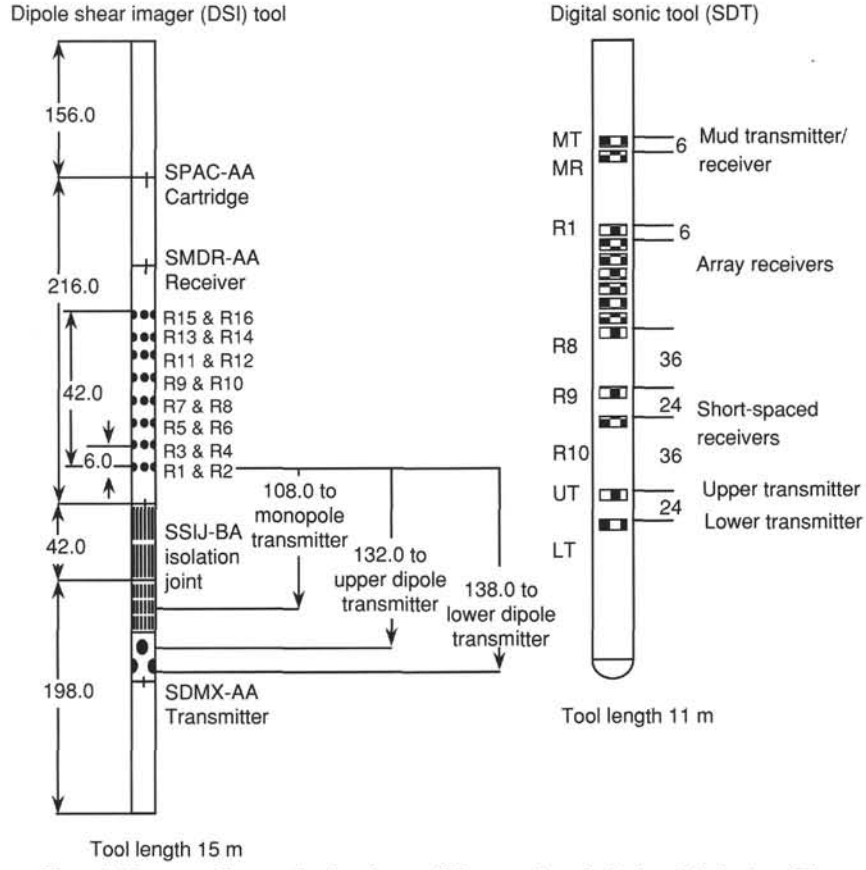

Figure 9. Summary diagram showing the two different sonic tools deployed during Leg 151.

Table 3. Summary of logging tool specifics and their applications.

Tool	Acronym	Principle	Usable through pipe	Possible tool strings[h]	Synthetic seismogram[a]	Lithology mineralogy[b]	Porosity	Geochemistry elements	Other	Used on Leg 151	Typical data available on ship
Sonic	LSS/SDT BHC	Traveltime of sound (2 receivers)	N	1	G	F	G			N	
	SDT-C DSI	Traveltime of sound (8–10 receivers)	N		VG	F	G		c	Y	Velocity
Resistivity											
Shallow	SFL	Focused current	N	1	F	F	VG			Y	Resistivity
Medium	ILM	Induced current	N	1	F	F	VG			Y	Resistivity
Deep	ILD	Induced current	N	1	F	F	VG			Y	Resistivity
Gamma ray	GR	Natural γ-ray emissions	N	1	P	VG				Y	Gamma-ray counts
Caliper	MCD	Hole diameter	N	1		P			d	N	
Dual laterolog	DLL	Resistivity to current	N		F	F	VG			N	
Neutron porosity	CNTG	Absorption of bombarding neutrons	Y	1, 2	P	F	VG	H		Y	Porosity
Spectral γ-ray	NGT	Natural γ-ray emissions	Y	1, 2, 3, 4	P	VG		K, Th, U		Y	K, Th, U abundances
Bulk density	HLDT	Absorption of bombarding γ-rays	N	1, 2, 3	G	G	G			Y	Density
Induced γ-ray spectroscopy	GST	Capture of bombarding neutrons	Y	3	F	VG	F	Ca, Si, Fe,S,Ti, Gd, H, Cl		Y	Relative elemental yields
Al activation clay tool	AACT	Absorption of bombarding neutrons	Y	3	P	F	P	Al, Mn		Y	Aluminum abundance
Formation MicroScanner	FMS	Focused microcurrent	N	4	P	P	G		e	Y	Resistivity images, 2-axis caliper
12-channel sonic	MCS	Traveltime of sound (12 receivers)	N		VG	F	G		c	N	
Borehole televiewer	BHTV	Traveltime + reflectivity of borehole wall	N		P	F			f	N	
3-axis magnetometer	GPIT	Oriented magnetic field including inclination	N	1, 2, 3, 4	P	F			g	Y	Hole dip, inclination
Temperature	TLT	Formation temperature	Y	1, 2, 3, 4						Y	Temperature

Note: Usefulness of tool for application: VG = very good; G = good; F = fair; P = poor; Y = yes; N = no.

[a] Logs other than sonic and density can be converted to pseudosonic/density, based on known log responses to lithology and porosity.

[b] Percentages of minerals with abundance >3% are determined from simultaneous inversion of several logs.

[c] Shear velocity, apparent attenuation.

[d] Quality control for other logs.

[e] Detailed mapping of fractures, faults, foliations, and formation structures; analysis of depositional environments; formation dip.

[f] Stress directions, fracture orientation, structural dip, formation morphology.

[g] Magnetic reversals, stratigraphy, fault zones.

[h] See Figure 8.

for each element. The total counts recorded in each window, for a specified depth in the well, are inverted to give the elemental abundances of K (wt%), U (ppm), and Th (ppm). The NGT also provides a measure of the total gamma-ray signature (SGR or [K + U + Th]) and a uranium-free measurement (CGR or [Th + K]).

The natural gamma-ray measurement is commonly used to estimate the clay or shale content due to the relatively high abundance of radioactive elements in clay minerals. There are rock matrices, however, for which the radioactivity ranges from moderate to extremely high values because of the presence of volcanic ash, potassic feldspar, or other radioactive minerals.

High-temperature Lithodensity Tool (HLDT)

The HLDT uses a ^{137}Ce gamma-ray source and measures the resulting gamma-ray flux at fixed distances from the source. The radioactive source and detector array is pressed against the borehole wall by a strong spring arm. Excessive roughness or borehole width can cause some drilling fluid to infiltrate between the detector and the formation and cause density reading to be artificially low. Under normal operating conditions, attenuation of gamma rays is primarily caused by Compton scattering (Dewan, 1983), which is related to electron density. Formation density is inferred from this gamma-ray flux by assuming a direct relationship between electron density and bulk density, and also that the ratio of atomic weight and the atomic number for most common rock-forming elements is constant (about 2:1).

The photoelectric absorption effect is used as an indicator of matrix lithology that is independent of porosity. Photoelectric absorption occurs at gamma-ray energies below which Compton scattering can usually occur (<100 keV). The probability of photoelectric absorption occurring is dependent on the atomic number of a formation (e.g., more sensitive to elements with higher atomic numbers).

Sonic Tools

Sonic tools measure the difference in compressional-wave traveltimes between a transmitter and receiver. This provides a direct measure of vertical traveltime of sound in the adjacent formation (the interval traveltime [delta T]). It is used to calculate the porosity of the formation and sonic velocity.

Table 4. Approximate vertical resolution of various logging tools used during Leg 151.

Tool	Vertical resolution	Depth of investigation*
Phasor induction tool (DIT)		
ILD deep resistivity	200 cm, 88 cm, 59 cm	1.5 m
ILM medium resistivity	150 cm, 88 cm, 59 cm	76 cm
SFL shallow focussed	59 cm	38 cm
Natural gamma tool (NGT)		
	46 cm	Variable
	15–30 cm	
Lithodensity tool (HLDT)		
Density, photoelectric effect	49 cm (6-in. sampling)	Variable
	35 cm (2-in. sampling)	15–60 cm
	20 cm Alpha processing	
	30 cm Alpha processing (2 in.)	
Dipole shear imager (DSI)		
	30 cm	Variable
	Special processing 15 cm	10–60 cm
Sonic digital tool (SDT-C/array)		
	30 cm	Variable
	Special processing 15 cm	10–60 cm
Gamma-ray spectroscopy tool (GST)		
	75 cm	Variable
		12–20 cm
Aluminum activation clay tool (AACT)		
	25 cm	Variable
	12–20 cm	
Dual porosity compensated neutron tool (CNT-G)		
	55 cm (6-in. sample)	Variable and porosity dependent (15–60 cm)
	33 cm Alpha processing (6-in. sample)	
	25.4 cm Alpha processing (2-in. sample)	
Formation MicroScanner (FMS)		
	6 mm	5–25 cm
Lamont temperature tool (TLT)		
	(a) fast-response (1 s time constant reading)/s; (b) slow-response, high-accuracy reading (10 s time constant)/10 s; vertical resolution depends on logging speed.	

Notes: Standard sampling is at 15-cm (6-in.) intervals. High-resolution sampling is at 5.5-cm (2-in.) intervals. Alpha processing is a special high-resolution processing routine. *Depth of investigation is formation and environment specific; these depths are only rough estimates/ranges.

Sonic Digital Tool (SDT)

The SDT-C sonic tool acquires a digitized full sonic waveform downhole and at interval traveltimes. It has two transmitters and receivers with a 1-m spacing in addition to a linear array of eight receivers spaced at 15 cm, with a transmitter-receiver distance starting at 3.33 m (see Fig. 9). The digitally recorded full waveform is used post-cruise to determine shear wave and Stoneley wave velocities in addition to the real-time compressional velocity. Standard vertical resolution is 60 cm, although special array processing can produce a 15-cm resolution.

Dipole Shear Sonic Imager (DSI)

The DSI sonic tool was run during Leg 151. The DSI consists of one dual-frequency monopole transmitter (14 and 1 kHz) and two pairs of dipole transmitters (2.2 kHz). The dipole transmitters create a unidirectional flexing of the borehole wall that excites shear waves in contrast to a "nondirectional" monopole source. The receiver consists of an array of eight receiver groups with a 15-cm spacing. Within each receiver group, there are four receivers in line with the dipole transmitters (see Fig. 9). The DSI can measure compressional and Stoneley wave velocities, but also can directly measure shear wave velocity in a "soft" formation (where the shear wave velocity is less than the velocity of the drill fluid, e.g., poorly lithified sediment). Besides the conventional first-motion detection methods, DSI uses digital correlation analysis between signals from the receiver array to determine wave propagation velocities. Full waveforms are digitally recorded for post-cruise analysis.

Geochemical Tool String Combination

The geochemical logging tool string (GLT) consists of four separate logging tools: the natural gamma-ray spectrometry tool (NGT*), the compensated neutron tool (CNT*), the aluminum activation clay tool (AACT*), and the gamma-ray spectrometry tool (GST*), shown in Figure 8. These four tools use three separate modes of gamma-ray spectroscopy for a comprehensive elemental analysis of the formation. The NGT is located at the top of the tool string so that it can measure the naturally occurring gamma rays from the radionuclides thorium (Th), uranium (U), and potassium (K) before the formation is irradiated by the nuclear sources contained in the lower tools (Fig. 8). The CNT, located below the NGT, carries a californium (^{252}Cf) neutron source to activate Al atoms in the formation. The AACT, a modified NGT, is located below the ^{252}Cf source, measuring the gamma rays from activation in addition to the natural gamma-ray activity of the formation. By combining the AACT measurement with the previous NGT measurement, the background radiation is subtracted and a reading of formation Al is combined (Scott and Smith, 1973). The GST, at the base of the string, carries a pulsed neutron generator to induce prompt-capture gamma-ray reactions in the borehole and formation and a NaI(TI) scintillation detector to measure the energy spectrum of the emitted gamma rays. As each of the elements in the formation is characterized by a unique spectral signature, it is possible to derive the contribution (or yield) of each of the major elements silicon (Si), iron (Fe), calcium (Ca), titanium (Ti), sulfur (S), gadolinium (Gd), and potassium (K), from the measured spectrum and, in turn, to estimate the relative abundance of each in the formation when combined with the elemental concentrations from the NGT and AACT. The GST also measures hydrogen (H) and chlorine (Cl) in the borehole and formation, although these elements are not used for determining the rock geochemistry.

The only major rock-forming elements not measured by the geochemical tool string are magnesium (Mg) and sodium (Na); the neutron-capture cross section of these elements is too small relative to their typical abundances to be detected by the GLT. A rough estimate of Mg + Na can be made in some instances by using the photoelectric factor (PEF), measured by the lithodensity tool (Hertzog et al., 1989). This calculation was not implemented on the geochemical data from Leg 151 as the (Mg + Na) component was below the detection resolution of this technique (Pratson et al., 1993).

Dual Porosity Compensated Neutron Tool (CNT-G)

The CNT-G consists of an AmBe neutron source and a set of two neutron detectors designed to measure neutrons of two different energies (thermal and epithermal neutrons). The radioactive source emits high energy neutrons (4 MeV) into the formation that are scattered and slowed by collisions with other nuclei. Because neutrons have an atomic mass similar to that of hydrogen, most neutron slowing is caused by collisions with hydrogen, almost all of which resides in water molecules. Changes in the number of neutrons detected at a receiver can thus be related to porosity. Because water is present both in pores and as bound water (e.g., in clay minerals), porosities measured in the presence of hydrous minerals are often overestimates of true porosity. This can be alleviated by comparing epithermal and thermal neutron porosities (Ellis, 1987). The accuracy of neutron porosity may be adversely affected by variations in hole size, which result in an increased H proportion from the drill fluid.

*Trademark of Schlumberger.

Formation MicroScanner (FMS)

The FMS tool produces high-resolution microresistivity images of the borehole wall that can be used for detailed sedimentological or structural interpretations. The tool consists of 16 electrodes, or "buttons," on each of four orthogonal pads. These four pads are pressed against the borehole wall. Pad electrodes are spaced about 2.5 mm apart and are arranged in two diagonally offset rows of eight electrodes each (Fig. 8). A focused electrical current flows between buttons and is recorded as a series of logs that reflect the microresistivity variations of the formation. Processing converts the measurements into spatially oriented images of the borehole wall using information from the general purpose inclinometer tool (GPIT). Further processing can provide oriented measurements of strike and dip of planar features. The vertical resolution of the FMS is about 6 mm. Coverage is restricted to about 22% of the borehole wall for each pass of the tool. Use of the FMS is restricted to hole diameters of less than 37 cm. Thus, no useful information can be obtained from washed-out hole sections.

Lamont-Doherty Temperature Tool (TLT)

The TLT is a self-contained temperature recording tool that can be attached to any Schlumberger tool string. Data from two thermistors and a pressure transducer are collected at a pre-determined interval between 0.5 and 5 s and stored within the tool. Following the logging run, data are transferred from the tool to a shipboard computer for analysis. A fast-response, lower accuracy thermistor is able to detect sudden temperature excursions caused by fluid flow from the formation. A slow-response, higher accuracy thermistor can be used to estimate borehole fluid temperature. If the history of drill-fluid circulation in the hole and at least two temperature logs are available (Jaeger, 1961), the post-drilling equilibrium geotherm can be estimated. Conversion to depth is based on pressure recordings from the pressure transducer and from the Schlumberger unit elapsed time (ETIM) records.

Log Data Quality

Log data quality may be seriously degraded by rapid changes in the hole diameter and in sections where the borehole diameter is greatly increased or washed out. The result of these effects is to impair logging by causing "bridging" or "tool sticking" and to increase the fluid volume between the formation and the logging tool. Deep investigation devices such as resistivity and velocity tools are least sensitive to borehole effect. Nuclear measurements (density, neutron porosity, and both natural and induced spectral gamma ray) are more sensitive due to their shallower depth of investigation and because of the effect of increased drill-fluid volume on neutron and gamma-ray attenuation. Corrections can be applied to the original data to reduce these effects, provided that the washout is not large.

By use of the NGT on each string, data can be depth correlated between logging runs. Logs from different tool strings, however, may still have minor depth mismatches caused either by cable stretch or ship heave during recording. Small errors in depth matching can impair the multilog analyses in zones of abruptly varying lithology. Ship heave is minimized by a hydraulic wireline heave compensator designed to adjust for rig motion during logging operations.

Log Analysis

During each logging run, incoming data are observed in real time on a monitor in the Maxis logging unit and simultaneously recorded on disk in the Schlumberger logging unit. After logging, data are processed and reformatted with the Terralog log-interpretation software package. FMS data are processed post-cruise at IMT (France), and the geochemical data at the University of Leicester (England), both under the direction of the Borehole Research Group at LDEO.

Calculation of Porosity and Density Profiles from Resistivity Logs

During Leg 151 the resistivity log was commonly used to calculate a sediment porosity profile, to compare with the shipboard physical properties data, and to estimate sediment wet-bulk density. Porosity can be determined from the resistivity logs by using the Archie equation (Archie, 1942):

$$S_w^{\,a} = (a/f^{m})\,(R_w / R_t) \tag{10}$$

where S_w is the water saturation, equal to 1 for these virtually hydrocarbon-free sediments, R_w is the resistivity of the formation water, f is the fractional porosity, R_t is the measured formation resistivity, and both a and m are constants depending on lithology and pore space geometry.

At many Leg 151 sites density measurements from the logs were poor because of bad hole conditions. For this reason, a density log was commonly estimated from a resistivity log. The inversion process first consisted of creating a porosity profile and using this to estimate wet-bulk density. As the grain density was essentially constant at 2.7 g/cm^3, an estimated wet-bulk density could be calculated easily from:

$$\rho_b = \rho_w(\phi) + \rho_g\,(1 - \phi) \tag{11}$$

where ϕ is porosity, ρ is density, and the subscripts b, w, and g refer to that of bulk, water, and grains, respectively.

Synthetic Seismograms

Synthetic seismograms are generated from an impedance log. The interval transit time log (from the DSI and SDT tools) and density log (from the HLDT tool) are used to generate an impedance log (Gal'perin, 1974). The impedance vs. depth logs ar then converted to impedance vs. two-way traveltime and convolved with a zero-phase Ricker wavelet and various other digitized wavelet samples acquired from the *JOIDES Resolution* seismic source. The dominant frequency of the wavelet is varied depending on the source used in the original seismic profile. The vertical resolution of a 30-Hz wavelet is about 25–30 m (depending on interval velocity), so reflectors cannot generally be attributed to smaller-scale lithologic horizons (less than 30 m). The final synthetic seismogram calculated includes interbed multiples.

ONSHORE LOG PROCESSING[3, 4]

Standard Log Processing

Additional log processing and display were performed post-cruise, using Schlumberger "Logos" software and additional programs developed by members of the Borehole Research Group (BRG). Displays of most of these processed data appear with accompanying text at the end of the appropriate site chapters in this volume. Files of all processed logs (including FMS, dipmeter, and BRG temperature data not shown in printed form) plus explanatory texts are included on the CD/ROM disk enclosed in the back pocket of this volume; a directory of the contents of the disk is found at the front of this volume.

Shore-based processing of data from each hole consisted of: (1) depth adjustments of all logs to a common measurement below the sea floor; (2) corrections specific to certain tools; and (3) quality control and rejection of unrealistic values.

[3]James F. Bristow, Borehole Research Department of Geology, University of Leicester, Leicester, LEI 7RH, England.

[4]Cristina Broglia, Lamont-Doherty Earth Observatory, Columbia University, Palisades, NY 10964, U.S.A.

The depth shifting procedure is based on an interactive, graphical depth-match program that allows the processor to visually correlate logs and define appropriate shifts. The reference log and the log to be adjusted in depth are displayed side-by-side on a screen, and vectors connect the two at positions chosen by the user. The total gamma ray curve (SGR) from the NGT tool run on each logging string was used in most cases to correlate the logging runs. In general, the reference curve is chosen on the basis of constant, low cable tension and high cable speed (tools run at faster speeds are less likely to stick and are less susceptible to data degradation caused by ship heave). Other factors, however, such as the length of the logged interval, the presence of drill pipe, and the statistical quality of the collected data (better statistics are obtained at lower logging speeds) are also considered in the selection. A list of the amount of differential depth shifts applied at each hole is available upon request to BRG (LDEO) and in the "dshift.doc" file on the enclosed CD-ROM disk.

Specific tool corrections were performed on the gamma-ray data to account for changes in borehole size and for the composition of the drilling fluid. Processing techniques unique to the ACT and GST tools of the geochemical string are described in detail below.

Quality control was performed by cross-correlation of all logging data. If the data processor concluded that individual log measurements represented unrealistic values, the choices were to either discard the data outright and substitute the null value of "–999.25," or identify a specific depth interval containing suspect values that must be used with caution. The latter are noted in the text that accompanies all processed log displays. Quality control of the SDT acoustic data was based on discarding any of the four independent transit time measurements that were negative or that fell outside a range of reasonable values selected by the processor.

Locally, some intervals of log data appeared unreliable (usually due to poor hole conditions) and were not processed beyond what had been done onboard the ship. In general, a large (>12 in.) and/or irregular borehole affects most recordings, particularly those that require eccentralization (CNTG, HLDT) and a good contact with the borehole wall. Hole deviation can also degrade the data; the FMS, for example, is not designed to be run in holes that are more than 10° off vertical, as the tool weight might cause the caliper to close.

Geochemical Processing

Data Reduction

The well-log data from the Schlumberger tools are transmitted digitally up a wireline and are recorded and processed on the *JOIDES Resolution* in the Schlumberger Cyber Service Unit (CSU). The results from the CSU are made available as "field logs" for initial shipboard interpretation. Subsequent reprocessing is necessary to correct the data for the effects of fluids added to the well, logging speed, and drill-pipe interference. Processing of the spectrometry data is required to transform the relative elemental yields into oxide weight fractions.

The processing is performed with a set of log-interpretation programs written by Schlumberger, but these have been slightly modified to account for the lithologies and hole conditions encountered in ODP holes. The processing steps are summarized below:

Step 1: Reconstruction of Relative Elemental Yields from Recorded Spectral Data

This first processing step compares the measured spectra from the GST with a series of "standard" spectra to determine the relative contribution (or yield) of each element. These "standards" approximate the spectrum of each element. Using a weighted, least-squares inversion method, the relative elemental yields are calculated at each depth level.

Six elemental standards (Si, Fe, Ca, S, Cl, and H) are used to produce the shipboard yields, but three additional standards (Ti, Gd, and K) can be included in the post-cruise processing to improve the fit of the spectral standards to the measured spectra (Grau and Schweitzer, 1989). Although Ti, Gd, and K often appear in the formation in very low concentrations, they can make a large contribution to the measured spectra because they have large neutron-capture cross sections. One ppm of Gd in a sample, for example, will capture as many neutrons as 30.6% Si (Hertzog et al., 1989). Therefore, including Gd is necessary when calculating the best fit of the standard spectra to the measured spectrum, even though its typical abundance is only a few ppm.

The elemental standards (Si, Ca, Fe, Ti, Gd, K, Cl, and H) were used in the spectral analysis step for Holes 907A and 911A. The spectral standard for S was not used because this element exists in concentrations below the detection resolution of the tool in these holes; its inclusion in the spectral inversion would significantly increase the noise level in the other elemental yields. A linear 7-point (1.05 m) moving average was applied to the output elemental yields to increase the signal to noise ratios.

Step 2: Depth-shifting

Geochemical processing involves the integration of data from the different tool strings; consequently, it is important that all the data are depth-correlated to one reference logging run, as discussed earlier. The NGT gamma-ray log from the FMS tool string was chosen as the reference run in Hole 907A, and that from the geochemical tool string was used for Hole 911A.

Step 3: Calculation of Total Radioactivity and Th, U, and K Concentrations

The third processing routine calculates the total natural gamma-ray radiation in the formation, as well as concentrations of Th, U, and K, using the counts in five spectral windows from the NGT (Lock and Hoyer, 1971). This routine resembles shipboard processing, but the results are improved during post-cruise processing by including corrections for hole-size changes and temperature variations. A Kalman filtering (Ruckebusch, 1983) is used in the CSU processing at sea to minimize the statistical uncertainties in the logs, which can otherwise create erroneous negative values and anti-correlations (especially between Th and U). An alpha filter has been introduced more recently and is now recommended by Schlumberger for shore-based processing. This filter strongly smoothes the raw spectral counts but keeps the total gamma-ray curve unsmoothed before calculating out the Th, U, and K components. The outputs of this program are K (wet wt%), U (ppm), and Th (ppm), as well as total gamma-ray and computed gamma-ray (total gamma ray minus U contribution). The results of this process are shown in the summary logs at the end of each site chapter.

Step 4: Calculation of Al Concentration

The fourth processing routine calculates the concentration of Al in the formation using four energy windows recorded on the AACT. During this step, corrections are made for natural radioactivity, borehole-fluid neutron-capture cross section, formation neutron-capture cross section, formation slowing-down length, and borehole size.

Porosity and density logs are needed as inputs into this routine to convert the wet-weight percentages of K and Al curves to dry-weight percentages. Porosity logs were calculated from the deep induction and bulk density logs in both Holes 907A and 911A. The comparison of log-derived porosities with shipboard core measurements provided relatively poor correlation in both wells. As a result the porosity curve used in the geochemical processing consisted of interpolated core measurements, which were densely spaced, and comprehensively covered the logged section of both Holes 907A and 911A.

A correction is also made for Si interference with Al; the ^{252}Cf source activates the Si, producing the aluminum isotope, ^{28}Al, (Hertzog et al., 1989). The program uses the Si yield from the GST to determine the Si background correction. The program outputs dry-weight percentages of Al and K, which are combined in the next pro-

cessing step with the GST-derived elemental yields in the oxide closure model.

Step 5: Normalization of Elemental Yields from the GST to Calculate the Elemental Weight Fractions

Relative concentrations of the GST-derived elemental yields can be determined by dividing each elemental yield by a relative spectral sensitivity factor (S_i). This factor is principally related to the thermal neutron-capture cross sections and also to its gamma-ray production and detection probability of each element (Hertzog et al., 1989). The relative elemental concentrations are related to the desired absolute concentrations by a depth-dependent normalization factor (F), as defined by the relationship:

$$Wt_i = FY_i / S_i \quad (12)$$

where Wt_i = absolute elemental concentration, and Y_i = relative elemental yield.

The normalization factor is calculated on the basis that the sum of all the elemental weight fractions is unity (100%). The closure model handles the absence of carbon and oxygen, which are not measured by this tool string, with the approximation that each of the measurable elements combines with a known oxide or carbonate. The dry-weight percentages of Al and K are normalized with the reconstructed elemental yields to determine the normalization factor at each depth interval from the following equation:

$$F(\Sigma_i X_i Y_i / S_i) + X_k Wt_k + X_{Al} Wt_{Al} = 100, \quad (13)$$

where

X_i = oxide factor; atomic weight of the associated oxide or carbonate of element i ÷ atomic weight of element i,
X_k = oxide factor; atomic weight K_2O ÷ atomic weight of K,
Wt_k = dry weight percentage of K as determined from the NGT,
X_{Al} = oxide factor; atomic weight of Al_2O_3 ÷ atomic weight of Al, and
Wt_{Al} = dry wt% of Al, as determined from the AACT.

The value X_i accounts for the C and O associated with each element. Table 5 lists the oxide factors used in this calculation for Holes 907A and 911A. After initially running this processing step, it was found necessary to further smooth the input geochemical yields to increase the signal to noise ratio. The elemental yields in both holes were smoothed by a linear 10-point (1.52 m) moving average and the input Al and K data by a 5-point (0.76 m) moving average in Hole 907A and 7-point (1.05 m) moving average in Hole 911A. In addition, after initially running the oxide closure model, the initial wt% Ca in Hole 907A was found to be zero in the entire open hole section. To improve the statistics of the other elements, the Ca elemental yield was redistributed to the other elements (Grau and Schweitzer, 1989). Following these steps of smoothing and redistribution, the oxide closure model was run again.

Table 5. Oxide factors used in normalizing elements to 100% and converting elements to oxides.

Element	Oxide/ carbonate	Conversion factor
Si	SiO_2	2.139
Ca	CaO	1.399
Fe	FeO*	1.358
K	K_2O	1.205
Ti	TiO_2	1.668
Al	Al_2O_3	1.889

Step 6: Calculation of Oxide Percentages

This routine converts the elemental weight percentages into oxide percentages by multiplying each by its associated oxide factor, as shown in Table 5 (with the exception of Ca in Hole 907A).

Shipboard X-ray fluorescence measurements are shown for comparison to the GST-derived oxides in the logging figures, located at the end of the "Site 907" and "Site 911" chapters.

Step 7: Calculation of Error Logs

The calculated statistical uncertainty of each element is calculated for each of the elements measured with the GST and NGT (Grau et al., 1990; Schweitzer et al., 1988). This error is strongly related to the normalization factor, which is calculated at each depth level (Equation 13). The statistical uncertainty of the elements is displayed in the above-mentioned logging figures along with the normalization factor. A lower normalization factor represents better counting statistics and therefore higher quality data.

Ms 151IR-102